Donelan

Environment Canada
Environnement Canada

National Water Research Institute
Institut National de Recherche sur les Eaux

BRAGG-SCATTERING AND EQUILIBRIUM RANGES IN WIND-GENERATED WAVES - WITH APPLICATION TO SCATTEROMETRY

by
Mark A. Donelan[1] and Willard J. Pierson Jr.[2]

Inland Waters Directorate
Direction Générale des Eaux Intérieures

This manuscript has been submitted to the

Journal of Geophysical Research - Oceans

for publication and the contents are subject to change

BRAGG-SCATTERING AND EQUILIBRIUM RANGES IN WIND-GENERATED WAVES - WITH APPLICATION TO SCATTEROMETRY

by

Mark A. Donelan[1] and Willard J. Pierson Jr.[2]

[1]Shore Processes Section
Hydraulics Division
National Water Research Institute
Canada Centre for Inland Waters
Burlington, Ontario, Canada L7R 4A6

[2]CUNY Institute of Marine
and Atmospheric Sciences
The City College
City University of New York
New York, N.Y., U.S.A.

August 1984

ABSTRACT

A composite divided scale model for radar backscatter from the ocean surface is constructed to meet the needs of scatterometry. The primary scattering mechanism is assumed to be Bragg scattering in which the normalized radar backscattering cross-section is proportional to the spectral density of the resonant Bragg water waves. The form of the equilibrium wavenumber spectrum is derived on the assumption that the short wave energy density reflects a balance between direct wind forcing and dissipation due to breaking and to viscosity. This theoretical equilibrium spectrum, which links the wave spectrum to the wind, is included in a Bragg scattering model, which links backscattering cross-section to the wave spectrum. The effects of tilt and modulation of the Bragg resonant waves by the longer waves are included and the model is tested against aircraft circle flight K_u-band radar backscatter measurements (in the wind speed range of 5.5 m/s to 20 m/s) with very encouraging results. The model is then exercised over a much wider wind speed range and also for C and L bands. It is demonstrated that at low wind speeds scatterometry is sensitive to surface water temperature through its effect on the viscous dissipation of short waves. For high wind speeds at anemometer height the backscattering cross-section becomes less sensitive to wind speed and at even higher speeds decreases as the wind speed increases. The wind speed at which this "roll-over" occurs is dependent on radar wavelength and incidence angle, being as low as 22 m/s for K_u-band at 25° incidence. This rather complicated wind speed dependence of radar backscatter contrasts strongly with the current power law models and helps explain many of the inconsistencies that have arisen in the analysis of scatterometer data to-date.

RÉSUMÉ

Un modèle composite à échelle divisée de la rétrodiffusion de signaux radar par la surface de l'océan est en construction pour répondre aux besoins de la diffusométrie. Le mécanisme de diffusion primaire est censé être une diffusion de Bragg dans laquelle la section normalisée de la rétrodiffusion radar est proportionnelle à la densité spectrale des vagues de Bragg en résonance. La forme du spectre d'équilibre des nombres d'onde est obtenue à partir de l'hypothèse que la densité d'énergie des vagues courtes reflète un équilibre entre le soulèvement de vagues par l'action directe du vent et la dissipation due à l'écroulement des vagues et à la viscosité. Ce spectre d'équilibre théorique, qui relie le spectre des vagues au vent, est inclus dans un modèle de la diffusion de Bragg, lequel met en relation la section de la rétrodiffusion et le spectre des vagues. Les effets du basculement et de la modulation des vagues résonantes de Bragg dus aux ondes plus longues sont inclus et le modèle est comparé aux résultats de mesures de la rétrodiffusion radar dans la base K_u effectuées au cours de vols circulaires (dans la gamme de vitesses des vents de 5,5 m/s à 20 m/s), avec des résultats très encourageants. Le modèle est ensuite essayé dans une gamme de vitesses de vent beaucoup plus étendue et dans les bandes C et L. Il est ensuite démontré qu'à de faibles vitesses du vent, la diffusométrie est sensible à la température de l'eau de surface à cause de son effet sur la dissipation visqueuse des vagues courtes. Pour de grandes vitesses du vent à hauteur d'anémomètre, la section de la rétrodiffusion devient moins sensible à la vitesse du vent et, même à des vitesses supérieures, la section diminue à mesure que la vitesse du vent augmente. La vitesse du vent à laquelle ce "renversement" se produit dépend de la longueur d'onde radar et de l'angle d'incidence, atteignant une valeur aussi basse que 22 m/s pour la bande K_u à 25° d'incidence. Cette dépendance complexe de la rétrodiffusion radar envers la vitesse du vent contraste fortement avec les modèles actuels de la loi de la puissance et permet d'expliquer un bon nombre des incohérences qui se sont produites dans l'analyse des données diffusométriques obtenues à ce jour.

MANAGEMENT PERSPECTIVE

This paper is very important for the development of global climate models which are essential for longer time weather forecasts and for the assessment of the "Greenhouse effect" on the world and Canadian climate and subsequently national water resources. Future management decisions in water resources will lean heavily on global climate models which in turn demand reliable global data to develop them. Global wind data over oceans, which are the thermodynamic "engine" driving the weather "machine" can only be obtained from weather satellites which are a scatterometer to observe the ocean surface. This paper gives a theory which permits the interpretation of the signal so that surface wind speeds and direction are deduced correctly. From the theory a model was developed and shown to be correct. Moreover, the theory permits improved interpretation of past scatterometer data. This theory and model will likely be implemented for satellites planned by U.S.A., Canada, Europe, and Japan in the next decade.

T. Milne Dick
Chief
Hydraulics Division

PERSPECTIVE DE GESTION

La présente étude est très importante pour la mise au point de modèles climatiques mondiaux, lesquels sont essentiels pour l'établissement de prévisions météorologiques sur une plus longue échéance et pour l'évaluation de l'effet de serre sur le climat mondial et canadien, et par conséquent sur les ressources en eau du pays. Les futures décisions de gestion en matière de ressources en eau reposeront fortement sur les modèles climatiques mondiaux, lesquels à leur tour exigeront des données fiables à l'échelle mondiale pour être mises au point. Les données éoliennes mondiales au-dessus des océans, qui sont les "moteurs" thermodynamiques entraînant la "machine" météorologique ne peuvent être obtenues qu'au moyen de satellites météorologiques, lesquels servent de diffusiomètres pour l'observation de la surface océanique. Dans la présente étude, l'auteur énonce une théorie qui permet d'interpréter le signal de telle manière que les vitesses et la direction du vent à la surface puissent faire l'objet d'une déduction juste. À partir de la théorie, un modèle a été mis au point et il s'est révélé juste. En outre, la théorie permet d'obtenir une interprétation améliorée des données diffusiométriques antérieures. Cette théorie et ce modèle devraient être intégrés aux satellites prévus par les États-Unis, le Canada, l'Europe et le Japon pour la prochaine décennie.

T. Milne Dick

Chef

Division de l'hydraulique

Introduction

The demonstration that satellite borne instruments can yield information on marine surface winds is an extremely important advance in remote sensing. (The stated objectives of the Seasat Satellite Scattermometer (SASS) program were met, at least in the range of wind speeds of 4 to 16 m/s). The instruments used for this purpose are active microwave devices operating at GHz frequencies, called scatterometers. To date efforts have been devoted to making anemometers of scatterometers by the empirical determination of transfer functions i.e. equations of the form $\sigma^o = \sigma^o (V, \chi, \theta)$, relating normalized backscattered power to some aspect of the surface wind vector (V, χ) and the radar incidence angle, θ. Most of the work has been based on regarding the surface wind (at 10 m or 19.5 m height) as the basic sensed variable (Moore and Fung, 1979; Jones et al. 1982; Pierson and Salfi, 1982 ; Schroeder et al. 1982a and 1982b; Pierson, 1983), though the friction velocity has not escaped attention (Jones and Schroeder, 1978; Liu and Large, 1981; Brown 1983).

In a recent paper Wojceshyn, et al. (1984a) have shown that the transfer (or model) functions used for horizontal incident-horizontal scattered polarization (electric field vector perpendicular to the plane of incidence, abbreviated HH) are inconsistent with those used for vertical-vertical polarization (abbreviated VV). The differences in estimated wind speeds are quite large (up to 5 m/s) and imply perhaps that the process of deducing the wind from the backscatter measurements was partially incorrect or that the model functions, σ^o_{VV} (V, χ, θ), and

σ^o_{HH} (V, χ, θ), were in error or that a combination of both caused the discrepancies. Both model functions were determined empirically in the same way - by assuming a power law wind speed dependence over a restricted mid-range of surface wind speeds (5 to 16 m/s) from the Joint Air-Sea Interaction (JASIN) program, for which good surface observations were available, and by using the then available National Aeronautics and Space Administration (NASA) circle flight data (Jones, Schroeder and Mitchell, 1977). The approach taken by Woiceshyn et al (1984a) is novel and very valuable for it avoids the slippery question of the quality or suitability of a particular set of surface data used in verifying the scatterometer's anemometry and demonstrates the internal inconsistency of the methods that were used.

The results of this internal HH-VV comparison, especially for strong winds, call for a new look at the basis for scatterometer-anemometry and Woiceshyn et al. attempt to provide one. Their approach relies heavily on the drag coefficient formulation of Kondo (1975) and Kondo et al. (1983) and on the existence of several ranges in the wind speed dependence of the drag coefficient. Apart from the fact that other careful measurements of oceanic surface stress (e.g. Smith, 1980, Large and Pond, 1981) show no such complex behaviour, the possibility of a unique relationship between stress and wind speed certainly depends on virtual constancy of the state of wave development (Kitaigorodskii and Volkov, 1965; Donelan, 1982). There is no unique relationship between $\bar{U}_{10}$ ($\bar{U}_{19.5}$), u_* and z_0 except perhaps when the wind generated seas are fully developed.

In a recent paper Donelan and Pierson (1984), hereafter referred to as DP1, demonstrate that the wind parameter most closely related to microwave Bragg scattering is the wind very near the surface at a height of order of the wavelength of the Bragg resonant water wave. Frequency spectra of short, but distinctly gravity waves (wavelength λ = 20.7 cm), are used

to support the analysis. The results are therefore of value in the interpretation of L band synthetic aperture data. In particular DP1 demonstrated that neither wind speed ($U_{19.5}$) nor friction velocity (u_*) is uniquely related to the spectral density when data for various states of wave development are considered. DP1 indicated a possible new approach to scatterometry, but did not attempt to verify the approach using actual backscatter observations.

In this paper (DP2) we extend the ideas presented in DP1 for frequency spectra to wave-number spectra, and employ the published results of many Bragg scattering experiments to verify them. Observational results on wave growth and physical reasoning lead to a form of the wave-number spectrum for capillary-gravity waves (wave-number $k = \frac{2\pi}{\lambda}$ in the range 10^{-1} to 10^{+1} cm $^{-1}$) which is in excellent accord with observations. The dependence of spectral density on surface wind is deduced and demonstrates that power law model functions are inadequate and will, when fitted to a mid range of surface data, underestimate the wind speed at both low and high speeds. A new composite model is constructed and the expected VV normalized backscatter cross section (σ^o_{vv}) is compared with the available observations. The results are shown to yield the observed microwave frequency, incidence angle, wind speed and direction dependence. However, the HH backscatter (σ^o_{HH}) is much more sensitive to white capping and wave steepness. It is suggested that σ^o_{HH} therefore needs more study for anemometry purposes . The difference of the observed ratio $\sigma^o_{HH}/\sigma^o_{vv}$ from that deduced from the model might be a useful measure of certain aspects of the wave field, in particular the r.m.s steepness and the degree of white capping.

Our results are a blend of theory and empiricism. The method of trying to fit backscatter to a power law for wind speed (or friction velocity) by regression techniques depends too much on empiricism and is incapable of coping with the very complex physical processes involved in the generation of an equilibrium wave spectrum for a given wind speed. This is especially true in attempting to understand the effects of viscosity, and to cover the entire range of radar wavenumbers from L band to K_u band. The power law assumption is the weak point of all previous efforts to relate backscatter to wind.

In this study, we obtain a theoretical form for the high wavenumber spectrum that requires some empirically determined constants. The theoretical equilibrium spectrum, which links the waves to the wind, is included in a Bragg scattering model, which links backscattering cross-section to the wave spectrum. Some quite dramatic results on the relationship between backscatter and wind emerge from this analysis.

Wind forcing:

Various attempts have been made to estimate the wind input to waves by measuring the pressure at or near the surface. The growth rates of the well known Bight of Abaco experiment (Snyder et al., 1981) are approximated by:

$$\frac{1}{\omega E}\frac{\partial E}{\partial t}\cdot\frac{\rho_w}{\rho_a}=\frac{\beta}{\omega}\cdot\frac{\rho_w}{\rho_a}\sim(0.2\text{ to }0.3)\cdot(\mu_1-1);\ 1<\mu_1<4 \qquad (1)$$

where E is the energy spectrum E (ω), β is the exponential growth rate, ω the radian frequency, ρ_a, ρ_w air and water densities, $\mu_1 = U_5 \cos\theta/c$, c the phase speed, U_5 the mean wind at 5 m height, and θ the angle between propagation direction of waves and wind.

The more recent field experiments of Hasselmann et al. (1983) and Hsiao and Shemdin (1983) show a stronger than linear dependence of β/ω on $(\mu - 1)$. Hsiao and Shemdin's data cover a larger range of μ_2 ($1<\mu_2<7.4$) than the previous field experiments and they find that β/ω depends quadratically on $(\mu_2 - 1)$.

$$\beta/\omega\cdot\frac{\rho_w}{\rho_a}=0.12\,(\mu_2-1)^2;\ 1<\mu_2<7.4 \qquad (2)$$

where $\mu_2 = 0.85\, U_{10} \cos\theta/c$.

Hsiao and Shemdin (1983) point out that within experimental scatter (2) is an adequate representation of the data which led to (1).

Plant (1982) has shown that β/ω values from several laboratory and field experiments are quadratically dependent on μ_* ($= u_* \cos^{1/2}\theta/c$) over a wide range of μ_*

$$\frac{\beta}{\omega} = 0.04\ \mu_*^2 \qquad (3)$$

in agreement with the theory of Miles (1959). However this relationship fails at small values of μ_* corresponding to μ_1, μ_2 near 1.

Hsiao and Shemdin (1983) include their relationship (2) in Plant's (1982) summary plot of β/ω vs u_*/c and demonstrate that (2) models β/ω well at low values of μ_*. However, at high values of μ_* (2) overestimates most of the measurements. This overestimate arises because Hsiao and Shemdin use the equivalent 10 m wind U_{10} even for the laboratory data obtained in tanks of height 1 m or so in which the waves corresponding to very high μ_* have wavelengths of 10 cm or less. We will demonstrate below that this and other difficulties are cleared up by a more logical choice of wind speed.

The weight of experimental evidence has shifted towards an expression of the form of (2) to describe wind forcing of water waves. This, of course, has the character of wind input due to form drag - an idea first expounded by Jeffreys (1924, 1925). If the mechanism of wind input to waves is indeed analogous to form drag on a rough wall, then the appropriate reference wind is not that at the "critical height" (Miles, 1957) but instead at some height above the roughness elements, and related to their scale. In a recent numerical calculation Al-Zanaidi and Hui (1984) obtain a result of the form of (2) but in which U_λ is used instead of U_{10}. The choice of wavelength related height cannot be specified by rigorous argument. In this paper, we have chosen one half wavelength as the reference height since at this height the disturbance due to a particular wavelength (observed to be exponential by Snyder et al., 1981) has nearly vanished. At the same time this height is sufficient to clear even the steepest capillaries. $U_{\lambda/2}$ is thus our reference height or "U_∞" for the waves being considered.

Scatterometry is largely concerned with the capillary-gravity transition region of the spectrum where there nave been no successful measurements of surface pressure and thereby estimates of direct wind forcing. However, Larson and Wright (1975), in a splendid experiment, obtained the exponential growth rates of capillary-gravity waves following an abruptly turned-on wind. The growth rates have been ascribed to instability of interfacial laminar shear layers (Valenzuela, 1976), but for nearly all the duration of exponential growth the wave heights exceed the thickness of the laminar sub-layer in the air. As pointed out by Valenzuela (1976), the u_* values quoted by Larson and Wright (1975) are too large since they were measured at steady-state after the wave spectrum had attained its fetch limit. The exponential growth of the waves being considered (wavelengths in the range of 0.7 to 7 cm) is over in a matter of a few seconds, long before the fetch limit is reached. Thus, instead of the u_* values quoted by Larson and Wright, we use the mean of their (steady-state) values and the values corresponding to smooth flow (initial-state) i.e. $z_0 u_*/\nu = 0.137$; when z_0 and ν are the roughness length and kinematic viscosity of the air boundary layer. The steady-state values of u_* measured by Larson and Wright were: 27, 66, 124 cm/s; the values computed from the mean of the initial and final values were: 24, 53, 90 cm/s. Thus, the thickness of the laminar sub-layer δ ($= 11.5\ \nu/u_*$, Schlichting, 1968) varies from 0.07 to 0.02 cm. The theoretical maximum height/wavelength ratio for gravity waves is about 1/7 (Michell, 1893) while for capillary waves almost 3/4 (Crapper, 1957). However, Schooley's (1958) observations of waves in the capillary-gravity region show maximum height/wave-length ratios of 0.5. If we assume that the shortest waves observed by Larson and Wright ($\lambda = 0.72$ cm) attain a limiting height of 0.36 cm while the

longest (λ = 6.98 cm), which are almost gravity waves, are limited at about 1.0 cm. then, for the two extreme cases of smallest wave-deepest laminar layer and largest wave-shallowest laminar layer, the waves eventually exceed the depth of the laminar layer by factors of 5.1 and 50 respectively. Therefore, the wave crests would be above the laminar layer while the observed backscattered power (proportional to height squared, Wright, 1966) increased by 1.4 and 3.4 orders of magnitude respectively. Larson and Wright noted exponential growth in backscattered power over 2 - 5 orders of magnitude. It would seem then that the exponential growth observed by Larson and Wright was associated more with the characteristics of rough flow in the turbulent boundary layer than with the laminar instability of the sheared viscous sub-layer. In the following we examine their data from this point of view.

In order to obtain $U(\lambda/2)$ we need both u_* and $U(z)$ at any height in the logarithmic boundary layer. The exponential growth estimates were obtained at three fetches (1.0, 3.0 and 8.4 m), with most of the data gathered at the intermediate fetch. Therefore we use the profiles supplied by Larson and Wright at that fetch - their figure 11(b). From this we obtain $U(z)$ values of 4.9, 9.7 and 14.5 m/s at heights of 10.0, 11.5 & 13.4 cm. In Figure 1 we compare the exponential growth rates of Larson and Wright with $\mu_\lambda = (U(\lambda/2)/c(\lambda)) - 1$. The data are tightly clustered about the straight line given by:

$$\frac{\beta}{\omega} \cdot \frac{\rho_w}{\rho_a} = 0.0072\ \mu_\lambda^{2.33} \qquad (4)$$

The quadratic best fit is also shown. As remarked earlier, a quadratic relationship is associated with rough flow and the relationship of

Figure 1 is clearly, though not greatly, steeper than quadratic. It is worth noting that the roughness Reynolds numbers ($R_* = z_o u_*/\nu$) are, for the three u_* values given, 0.43, 2.23 and 11.3. The first of these corresponds to transitional roughness, the second is on the border between transitional and fully rough and the third is fully rough. It could well be, indeed it must be, that the dynamical roughness state influences the mechanism for form drag. Unfortunately, we are not aware of the results of any suitably designed experiments to clarify this point. However, for our present purposes it is enough to note that the growth rates of capillary - gravity waves are closely correlated with μ_λ, much better than with u_*/c (Figure 2) as suggested by Plant (1982) or with $U_{19.5}$ (Figure 3), the usual scatterometer "predictor", which was chosen for Seasat purposes because u_* could not be measured routinely by conventional instruments. A recent paper by Keller et al. (1984) provides additional evidence to support the choice of μ_λ over $U_{19.5}$ or u_*. Keller et al. made observations of X-band microwave backscatter from a tower under various wind and atmospheric stability conditions. The relative backscattering cross-section depended both on wind speed (measured at 24.7 m) and atmospheric stability as illustrated in their Figure 7. When they removed the wind dependence the relative cross-section varied much more strongly with stability than the estimated wind stress. The most unstable cases had relative cross-sections three times larger than would be expected from the stress. For a given wind speed at 24.7 m μ_λ is relatively large under unstable conditions since the wind gradient is relatively weak. The effect is quite pronounced since μ_λ is evaluated very close to the surface (for X-band at 45° incidence, $\lambda/2$ = 1.13 cm).

In this discussion of wind forcing we have assumed that the input to any particular wavenumber component of the spectrum is independent of the input elsewhere in the spectrum. The fact, that these short waves, so different from the spectral peak in wavenumber, are freely propagating under natural conditions (Donelan et al, 1984) tends to support this view, since phase coupling is necessary for effective wind forcing. The close agreement between the spectrally uncoupled parameter μ_λ and the observed growth rates suggests that the assumption is justified. Note that the experiments of Larson and Wright avoided the usual tank dilemma of unnaturally steep dominant waves with their attendant harmonic distortions by completing the measurements before they could develop.

In this paper we take the wind forcing for short waves under dynamically rough conditions to be that suggested by the quadratic fit to the data of Larson and Wright (Figure 1).

$$\frac{\beta}{\omega} \cdot \frac{\rho_w}{\rho_a} = 0.194 \quad \mu_\lambda^2 \tag{5}$$

Of course, this form of wind input acts only to amplify existing waves. The initiation of wavelets must be brought about by another process, perhaps an instability mechanism such as that suggested by Valenzuela (1976). However, we need not be concerned here with the initiation process since we are interested in the steady state in which appreciably steep waves are dissipating the energy supplied by the wind.

Spectral balance of short waves.

On the rear face of the spectrum, sufficiently far from the peak, the spectral balance may be dominated by wind input and dissipative processes, with other effects playing a lesser role. Several independent observations of radar backscatter from capillary-gravity waves provide strong evidence to support this contention as, indeed, do the optical slope measurements of Cox (1958). The evidence is in the appearance at low wind speed of a "dip" in the spectrum near the wavenumbers corresponding to the minimum in the dispersion relation and directed parallel to the wind. Valenzuela and Laing (1972) have shown that triad interactions may be possible and that they may cause a flux of wave energy from the slowest waves to their wavenumber neighbours. They claim that the dip in the spectrum is due to the energy drain from the slowest waves. Good examples of this are seen in the spectra of σ^0_{VV} from an aircraft over the North Atlantic in Valenzuela et al. (1971) or Guinard et al. (1971) and from tank data of σ^0_{VV} (Wright and Keller, 1971). In both cases the dip is noticeable only at light winds. Cox's (1958) optical slope measurements in a wave tank show the same effect. The obvious inference is that all but the lowest wind speeds the non-linear triad interactions are swamped by wind forcing and dissipation. At wind speeds above about 5 m/s it appears reasonable to assume that very short gravity waves ($\lambda < 30$ cm) and capillary waves aligned with the wind receive their energy from the wind and lose it through dissipative processes.

Early work that used theories due to Rice (1951) on modelling backscatter (e.g. Wright, 1968) was based on the concept (Phillips, 1958) of a fully saturated spectrum in the high wavenumber gravity and capillary wave region of the spectrum. That is, on the rear face of the spectrum the spectral density depends only on wavenumber. In such models as Wright's (1968) any wind dependence of radar backscatter must arise through the effects of the tilting of the Bragg scatterers by the longer waves and not by much change in the short wave density as a function of the wind speed as in Chia (1968), who extended what was then believed to be known about gravity waves too far into the capillary region.

It is now generally accepted that the rear face of the spectrum is not fully saturated, but is dependent on wind speed (Kitaigorodskii, 1983; Donelan et al. 1984). The actual wind speed dependence of the short waves is not available from measurements of frequency spectra because the difficulties of transforming the frequency spectra to wavenumber spectra are exacerbated by the doppler shifting due to (generally unknown) currents and the orbital velocities of longer waves. Wind speed dependent high frequency wave spectra were described by Pierson and Stacy (1973) for wind-wave flume experiments, including a very sharp increase in spectral density just above a certain u_*. The dependence on viscosity, which could cause the higher frequencies, or wave-numbers, to vary over a wider range was not noticed but is suggested by their Figure 5.1. The incorrect k^{-3} spectral form can be corrected by our new results.

Our approach here is to propose a spectral balance between wind input and dissipation which allows the high wavenumber spectrum to be wind speed dependent. Later we will insert this high wavenumber spectrum in a model which includes the effect of tilting of the long waves and compare the model's predictions with observations.

Dissipation:

The viscous dissipation of very short capillary waves has been worked out theoretically and verified experimentally by Mitsuyasu and Honda (1975) and Larson and Wright (1975), among others. It is a function only of wave-number k and ν the kinematic water viscosity. The spectral decay rate through viscosity is $\beta_\nu = 4\nu k^2$. This term is insignificant compared to the wind forcing for gravity waves and moderate winds. However, it increases rapidly with wave number and is believed to be the reason for the sharp spectral cut-off observed by Cox (1958).

The spilling of the crests of large gravity waves is clearly a major sink of wave energy. It depends strongly on spectral levels since no breaking occurs when the waves are not steep. A closer look at a wind driven sea reveals that the short gravity waves also break in a similar way, but the result is not spectacular and, without the production of foaming white caps, may even go unnoticed. The rate of dissipation of this "micro-breaking" is certainly dependent on spectral levels. Inasmuch as the dissipative region is locked to the wave crest and persists for a good fraction of a wave period, the energy loss is probably concentrated around the wave number of the breaking wave. Capillary - gravity waves appear to lose energy through the production of even shorter ripples at their crests, although the shortest waves are probably as much affected by the small scale turbulence created by larger waves breaking. In any case, the simplest assumption of an uncoupled (among wave numbers) dissipation seems a suitable starting point. By comparison with observation of the results so derived we will soon determine its adequacy. We define the normalized dissipation rate, β_d/ω

$$\frac{\beta_d}{\omega} = f_1 \left(\Psi(k, \bar{\theta}), k, \gamma, g\right) + \frac{\beta_\nu}{\omega} \qquad (6)$$

where $\Psi(k, \theta)$ is the polar wavenumber spectrum with $\theta = \bar{\theta}$ in the wind direction, γ is the surface tension/density ratio and g the gravitational acceleration. The viscosity, ν, is a strong function of temperature (Weast, 1970), whereas the surface tension is only weakly dependent on temperature and salinity.

Thus on dimensional grounds

$$\frac{\beta_d}{\omega} = f_1 \left[k^4 \Psi(k, \bar{\theta}); \frac{\gamma k^2}{g}\right] + \frac{\beta_\nu}{\omega} \qquad (7)$$

Noting that the function f_1 must have two asymptotic limits in the gravity and capillary ranges we adopt, for convenience, a power law behaviour for the function f_1 as in (8):

$$\frac{\beta_d}{\omega} = \alpha \left[k^4 \Psi(k, \bar{\theta})\right]^n + \frac{4\nu k}{c} \qquad (8)$$

where

$$\alpha, n = f_2, f_3 \left(\frac{\gamma k^2}{g}\right) = \begin{cases} \alpha_g, n_g \text{ for } \frac{\gamma k^2}{g} \ll 1 \\ \alpha_\gamma, n_\gamma \text{ for } \frac{\gamma k^2}{g} \gg 1 \end{cases}$$

the values of α and n are assumed to attain the asymptotic values of α_g, n_g and α_γ, n_γ in the gravity and capillary ranges of the spectrum. Long gravity waves lose energy largely by sudden breaking (generally "spilling" in deep water) while shorter (<10 cm) gravity waves and gravity-capillary waves appear to lose much of their energy to even shorter ripples formed at their crests when they steepen sufficiently. Perhaps the energy is passed to higher wave numbers and is eventually lost to viscosity (final term of (8)) in a Kolmogoroff-like cascade similar to that described by Kitaigorodskii (1983). The efficiency of this process increases with wavenumber so that purely capillary waves lose most of their energy in this way. The breaking process is far more critically dependent on wave steepness than the cascade process so that we would expect n_g to be larger than n_γ. Unfortunately sufficient data are not available to determine f_2 and f_3 or even their asymptotic limits. Most of the backscatter data correspond to Bragg scatterers in the gravity-capillary region. We will therefore assume that α and n are relatively constant over these wavenumbers and see how well that assumption allows the model to fit the observations.

Equilibrium ranges

Equating input (5) and dissipation (7) we obtain an expression for the downwind spectrum of the short waves in the "equilibrium" range.

$$\Psi(k, \bar{\theta}) = k^{-4} \left[\frac{0.194}{\alpha} \frac{\rho_a}{\rho_w} \mu_\lambda^2 - \frac{4\nu k}{\alpha c} \right]^{\frac{1}{n}} \tag{9}$$

$$= 0 \text{ when } [\quad] \text{ or } \mu_\lambda \leq 0$$

Here "equilibrium" is used formally to mean where wind input and dissipation are locally (with respect to wavenumber) balanced.

To our knowledge the only gravity-capillary wavenumber spectra that exist have been obtained by inverting measurements of microwave back scatter. It has been clearly established that the backscattered power for incidence angles well away from nadir and grazing (i.e. approximately 25^0 to 65^0) is due to Bragg resonance. See Valenzuela (1978) for a review. Wright (1966) has shown that the scattering cross-section is proportional to wave height squared of monochromatic waves. He later demonstrated (Wright and Keller, 1971; Keller and Wright, 1975) that first order Bragg scattering theory is appropriate in the capillary gravity region at mid-range incidence angles in the absence of longer and higher gravity waves that tilt the surface on which the "Bragg scatterers" ride. However, when a broad spectrum of waves exists the modulation of the Bragg scattering waves by the longer waves will alter the observed backscattered power. Thus, in order to interpret observed backscatter over a wind-generated sea, the spectrum (9) by itself is not sufficient. We must construct a model that includes the effects of the rest of the spectrum on the resonant Bragg waves insofar as these longer waves tilt the Bragg scatterers and produce variations in their heights over different phases of the longer waves. Such models have been called composite models.

A composite divided scale model.

Valenzuela (1978) has reviewed composite models in which the wave spectrum is divided into short Bragg scattering waves and longer waves whose principal function is to tilt the surface. In these models one is interested in the wave-number spectrum of the short waves and the probability distribution of slopes of the longer waves. Simple two-scale models like this require a more or less arbitrary decision regarding the separation of scales and generally assume that the waves of one scale are completely uncoupled from those of the other.

In this paper we draw on previous work on the slopes and energy distribution of gravity waves to construct a realistic two scale model. The parameters of the longer scale gravity waves - the "tilting waves", for short - can be tied down by observational results. By contrast, the only directional information available in the capillary-gravity range comes from Bragg scattering measurements, which at steady-state are necessarily made in the presence of tilting waves. The effects of the tilting waves are sufficiently large that such observational results can only be used to infer the wavenumber spectrum of the Bragg waves through a model which includes the effects of the tilting of the Bragg waves. Composite divided scale models provide the simplest approach to accounting for such effects. The unknown parameters of the short wave spectrum may therefore be inferred by adjusting them to yield good agreement between model and observations of radar scattering cross-section. In this model the principal parameters are α and n, the parameters discussed before. Two other relatively minor parameters ε and Γ, are discussed below. All other parameters are determined from the published results of other experiments.

The observations of Cox and Munk (1954), derived from sun glitter,

are still the most reliable observations of the slopes of natural wind waves. They found, in the range of wind speeds of 0.5 to 14 m/s and for long fetch, that : (a) the probability distribution of slopes is nearly Gaussian with, however, some skewness such that larger negative slopes occur than positive with the x-axis aligned with the wave propagation direction. (b) the variance of up/down wind slopes exceeds the variance of cross wind slopes by a factor between 1 and 2. (c) the up/down wind skewness increases with wind speed. (d) the kurtosis of the distribution of slopes is larger than Gaussian but only by an amount slightly larger than the estimated observational error. (e) the addition of an extensive oil slick to the surface reduces the variance of slopes by a factor of 2 or 3, eliminates the skewness and leaves the kurtosis unchanged. The oil slick appeared to remove virtually all waves shorter than 30 cm. Since the pioneering work of Cox and Munk several laboratory studies (e.g Cox, 1958, Keller and Wright, 1975 , Reece, 1978) have shown that the energy density of the ripples is related to the phase of the long waves. Longuet-Higgins (1983) has given theoretical arguments to show why this occurs and further pointed out that this is sufficient to explain the observed skewness of slopes, whereas harmonic distortion of the long waves is not. The addition of an oil slick attenuates the ripples and with them the skewness. In the context of our model we require a description of the modulation (in both amplitude and phase) of the energy density of the Bragg waves (ripples) by the longer tilting waves.

Cox (1958) showed that ripples were concentrated on the forward faces of the large waves but was not able to be more specific about the phase or amplitude of the modulation of the ripples with respect to the long waves. He also showed that the variance of slopes increased with wind speed. The tank photographs (Figure 18) of Mitsuyasu and Honda (1975) provide excellent documentation of the occurrence of ripples on the forward faces of the longer waves. Reece (1978) set about to explore the modulation in detail, but could only conclude that the distribution of energy density of the ripples

is modulated by up to 100 % of the mean (peak-to-peak) and the phase is advanced 45^{o} to 180^{o} with respect to the long waves. The modulation increases with wind speed. The results of Keller and Wright (1975) are in general agreement with this. The simplest modulation model which has these general features is one in which the modulation is simply proportional to upwind/downwind slope and is limited in the manner described by Reece.

$$\Psi(k,z_x) = \begin{cases} (1 - \varepsilon z_x)\,\Psi(k) & \text{for } |\varepsilon z_x| \leq \frac{1}{2} \\ (1 - 0.5\ \mathrm{sgn}\ (\varepsilon z_x))\,\Psi(k) & \text{for } |\varepsilon z_x| > \frac{1}{2} \end{cases} \tag{10}$$

where k is the wave number of the Bragg waves, z_x the downwind slope of the tilting waves and ε a constant to be determined empirically. The principal effect of this modulation will be to produce a difference in scattering cross section looking upwind versus downwind. The difference arises because looking upwind the enhanced waves are seen at an angle tilted towards the radar look direction (i.e. lower wave number and hence higher energy density) while the opposite is true looking downwind. The constant ε will be set by comparing the model output with observed upwind downwind differences in scattering cross section.

Cox and Munk (1954) have shown that the variance of slopes increases uniformly with wind speed and that much of the variance is due to waves of length less than 30 cm. For our purposes we need a spectral description of slopes and this has been provided by Cox (1958) for laboratory waves. The slope spectrum is inversely proportional to frequency above the peak frequency until it abruptly diminishes at about 70 Hz. The up/down wind slope variance due to waves in the frequency range ω_1 to ω_2 is therefore given by

$$\sigma_x^2 = G(U_{10}) \ln \left(\frac{\omega_2}{\omega_1}\right) \tag{11}$$

where $G(U_{10})$, derived from Cox's plots and tabulated values, is:

$$G(U_{10}) = 0.0014\, U_{10} - 0.003 \tag{12}$$

The quantity $G(U_{10})$ vanishes for a wind at 10 metres of 2.1 m/s. Such light winds, if constant, may be incapable of generating either gravity or capillary waves. Only swell and residual "dead" seas, generated locally by a previously higher wind, could be present in such areas. Backscatter would then be the result of the specular equation given later by equation (20).

The variance of cross wind slopes of the tilting waves is taken from the observations (with oil slick) of Cox and Munk. In the mean:

$$\sigma_y^2 = 0.86\, \sigma_x^2 \tag{13}$$

The lower limit of integration of the slope spectrum ω_1 depends on the state of wave development, since near full development the waves near the peak of the energy spectrum contribute very little to the slope variance. From the results of Donelan et al. (1984) we deduce that the reciprocal of the wave age should determine ω_1 and limit our present analysis to wind seas approaching full development as in (14) where c_p is the phase speed of the spectral peak. Our calculated results are all for U_{10}/c_p equal to one.

$$\omega_1 = 2\omega_p \qquad \text{for } U_{10}/c_p < 2 \tag{14}$$

The upper limit of integration ω_2 is simply the frequency of waves longer than the Bragg waves by a factor Γ. Thus using the theoretical dispersion relation:

$$\omega_2 = \left\{ \frac{gk}{\Gamma} \left(1 + \frac{\gamma k^2}{g\Gamma^2} \right) \right\}^{1/2} \tag{15}$$

The upper limit ω_2 must be sufficiently low so as to include only the waves long enough to tilt a group of Bragg waves more or less uniformly. This is the "separation of scales" parameter Γ and it is the final parameter set through tuning of the model to observations. Evidently, it should be such that, for ω_2, only waves somewhere between 10 and 100 times longer than the Bragg waves contribute to their tilting.

At low mean incidence angles occasional large tilts will reduce the local incidence angle to the point where specular reflection is important. We are therefore obliged to include calculations of the specular component as well.

Model structure

The composite model for Bragg-Specular scattering of the incident radiation k_0 is structured in the manner described by Valenzuela (1978), but with significant differences. At a given angle of incidence of the radar θ the Bragg wave number ($k = 2\ k_0 \sin\theta$) is computed and thus the variances of slopes of the tilting waves from(11) - (14). Then the double probability integral is evaluated in the ranges $\pm 4\sigma_x$ and $\pm 4\ \sigma_y$. Here our method diverges from the conventional methods described by Valenzuela (1978). The nearly Gaussian probability of slopes found by Cox and Munk, with slicks present, was obtained from bistatic measurements of sun glitter points on the sea surface with the sun as the radiation source and a special camera as the receiver. Geometrical corrections were made such that the slopes were effectively referred to the local vertical. This is not, of course, what the radar "sees" except at nadir. Thus, to account for the fact that a surface tilted towards the radar occupies a larger fraction of the field of view than a surface tilted away, we adjust the probabilities accordingly.

The correction can be shown to be:

$$p(z_x, z_y)_{radar} = \begin{cases} I \cdot p(z_x, z_y)_{Gaussian} \cdot \cos(\theta + \phi)/\cos\phi \\ 0 \quad \text{if } |\theta + \phi| \geq \frac{\pi}{2} \end{cases} \tag{16}$$

where θ is the incidence angle of the radar and ϕ is the angle of tilt of the surface in the plane of incidence. The second condition rejects from consideration all slopes turned normal or greater to the radar. $z_x = \tan\phi$, $z_y = \tan\delta$.

The value of I is chosen such that the sum of all probabilities of slopes seen by the radar is unity. A similar approach to adjusting the probability of seeing a particular slope has been taken by Chan and Fung (1977) except that they did not account for the invisibility (to the radar) of slopes such that $|\theta + \phi| \geq \pi/2$.

In establishing the limits of integration the values of $[\sigma_x]_\theta$ and $[\sigma_y]_\theta$ are set using (11) - (14) and θ the angle of incidence of the radar. However, as the surface tilts, the resonant Bragg wave continually changes and with it the range of wavenumbers that can contribute to any particular slope. Consequently the appropriate probability is not that associated with $(\sigma_{x,y})_\theta$ but rather that associated with $(\sigma_{x,y})_{\theta'}$, using (11) - (14):

$$p(z_x, z_y)_{Gaussian} = \frac{1}{2\pi[\sigma_x]_{\theta'}[\sigma_y]_{\theta'}} \exp\left\{-\frac{1}{2}\left(\frac{z_x^2}{[\sigma_x^2]_{\theta'}} + \frac{z_y^2}{[\sigma_y^2]_{\theta'}}\right)\right\} \tag{17}$$

where $\theta' = \cos^{-1}[\cos(\theta + \phi)\cos\delta]$ is the resultant angle of incidence.

This has a pronounced effect at small values of θ for as values of tilt on the edges of the distribution drive θ' and the Bragg wavenumber to very small values the corresponding energy density rises sharply and would artificially augment the modelled backscatter. Of course, the probability of large tilts affecting these longer waves is correspondingly smaller and (16) weights the contribution from these waves accordingly.

Near normal incidence the wavelength of the Bragg wave rises sharply. However, Bragg scattering is not effective when the heights of the scatterers become comparable with the wavelength of the incident radiation. We therefore impose a cut-off condition on the Bragg backscatter:

$$k_o a \leq 1 \tag{18}$$

where a is the standard deviation of the waves above the cut-off wavenumber. We use here the ω^{-4} equilibrium range of Donelan et al (1984), so that the cut-off frequency is given by:

$$\omega_c \geq (0.002\ k_o^2\ g\ U)^{1/3} \cdot (c_p/U_{10})^{0.15} \tag{19}$$

where c_p is the phase speed of the peak waves, so that c_p/U_{10} is the wave age.

In earlier sections we have dealt with the balance of wind input and dissipation in the wind direction and (9) describes the downwind spectral values. Of course, to complete the model we need a complete description of $\Psi(k, \theta)$. At large angles to the wind the wind input decreases rapidly and a balance between wind input and dissipation does not seem likely. Normal to the wind direction wind input vanishes but observations reveal significant energy density of the short waves. The natural variability of the

wind direction spreads the angular range of wind input beyond that which would occur in a laboratory tank with well defined wind direction. Nonlinear interactions among waves may also act to spread the energy beyond $\pi/2$. To account for this, though not to explain it, we assume as observed by Donelan et al. (1984) that the spectrum of the short waves spreads as $\text{sech}^2 \left\{ h_1 (\theta - \bar{\theta}) \right\}$ and h_1 is chosen to fit (9) at the peak ($\theta = \bar{\theta}$) and half-power points. If h_1 thus computed is greater than 1.24 it is set to 1.24 in keeping with the observations of Donelan et al. (1984).

The spectral balance (9) is such that, for each wave number there is a particular (water viscosity dependent) wind speed at which the spectrum vanishes. Of course, in any natural wind the instantaneous wind speed varies about a long term mean so that even when the mean wind is such that (9) vanishes, it may not during gusts. This is commonly observed at light winds in the appearance of patches of "cats-paws". To account for this in the model we allow the wind speed to have a Gaussian distribution about its mean with standard deviation proportional to the mean as observed by Smith (1974). The average value of Smith's observations over water of the standard deviation - to - mean ratio is 0.084 and this value is incorporated in our model. In fact, the streamwise component of boundary layer wind velocity fluctuations is somewhat skewed, but in the context of the model this is a minor correction and does not merit the extra computational effort. The principal effect of including wind gustiness in the model is to soften the low wind speed cut-off brought about by viscous dissipation. Otherwise for a given water temperature, T, there would be a very sharp drop, essentially to zero, as in Pierson and Stacy (1973), at that wind speed where (9) becomes zero. The measurements of Pierson and Stacy were made in a laboratory tank with steady winds. The gustiness was therefore much lower than that typical of the marine atmospheric boundary layer.

This completes the Bragg resonance part of the model. Finally as pointed out by Barrick and Peake (1968) we add the specular component which

following Valenzuela (1978) is:

$$\sigma^o_{spec} = \frac{|R(o)|^2 . \sec^4\theta}{2\,[\sigma_x]_\theta\,[\sigma_y]_\theta} \exp\left\{-\frac{\tan^2\theta}{2\,[\sigma_L^2]_\theta}\right\} \qquad (20)$$

where σ_L is the slope variance in the plane of incidence due to waves of wavenumber k_o/Γ and smaller. $[\sigma_x]_{k_o}$, $[\sigma_y]_{k_o}$ are the downwind and cross-wind standard deviations of these slopes. The reflection coefficient at normal incidence R(o) is known to depend on the small scale roughness (Yaplee et al. 1971). Since we are concerned largely with Bragg scattering and specular backscatter is a relatively minor correction at mid-range incidence angles, we approximate R(o) using the points given by Valenzuela (1978):

$$R(o) = 0{\cdot}55 \exp\left\{-13\,\sigma_H^2\right\} \qquad (21)$$

where σ_H^2 is the variance due to waves of wavenumber k_o and higher.

Comparative data.

The circle flights of the NASA C130 aircraft, using the radiometer scatterometer (RADSCAT), reported in Schroeder et al (1984) provide the most suitable data for tuning and testing the model. The cases used are the ones for which the authors state that the surface data from oceanographic ships, buoys or towers are the most reliable. The best regression fits to the circle data were consistently obtained with a model of the type

$$\sigma^o = \sum_{n=o}^{2} A_n \cos n\,\chi \qquad (22)$$

Equation (22) determines three parameters (A_0, A_1, A_2). The location of the minimum near 90^o is a function of A_1 and A_2 and depends solely on whether upwind backscatter is stronger than downwind, or vice versa, since setting the first derivative of (22) equal to zero yields (22a).

$$\text{Cos } \chi = \frac{A_1}{4A_2} \tag{22a}$$

The function σ^0 (V, χ, θ) is relatively flat near its maxima and minima, and the scatter of the original data make it virtually impossible to locate the minima within ± 20°, or so, of 90°. The backscatter values at 0°, 90° and 180° will be used in this paper and the actual location of the minimum near 90° will be a consequence of the properties of the wave spectra and slope probability distributions used in the model.

Since backscatter is proportional to the spectral components propagating in a direction parallel to the radar look direction either towards or away from it, then, if there were no upwind/downwind asymmetry, the minima would occur at exactly ± 90°. The fact that upwind is generally larger than downwind moves the minima closer to downwind. The degree of shift towards downwind depends on the upwind/downwind ratio (Figure 6) and is generally only a few degrees.

In Table I, we have summarized the values of the A's for the reliable cases, including only those with correlation coefficients squared, R^2, for vertical polarization in excess of one half. From these regressions the up, down and cross wind (χ = 0, π, ± π/2) values of σ^0_{VV} are computed and also listed in Table I. The values of α, n, ϵ and Γ are then adjusted to yield the best match between these observations and the model output, which is listed in Table II. The best values of the four empirically determined paramters α, n, ϵ and Γ are 150, 1.54, 1 and 40 respectively. The results are sensitive to choice of α and n and much less so to ϵ and Γ. As might be expected ϵ largely determines the up/down wind backscatter ratio and Γ affects the variance of tilts and hence, weakly, the wind dependence of the backscattered power.

Since the model requires the wind near the surface the results are to some extent dependent on the choice of drag coefficient. We have chosen to use the regression line given by Donelan (1982) which was modified from Garratt's (1977) summary of the measurements of many researchers by including only the direct measurements. This wind dependent drag coefficient ($C_D \times 10^3 = 0.96 + 0.041\ \bar{U}_{10}$) has been derived from measurements in the wind speed range of 4 m/s to 16 m/s. Our results throughout are based on a neutrally stratified atmosphere.

In Figure 4 we compare the model output to observations of upwind backscattering cross-section for vertical polarization, i.e., σ^o_{vv}. There are 24 data points and the four parameters of the model have been tuned to this data set leaving 20 degrees of freedom to test the model's performance. Angles of incidence of 19° and 67° are, in the mean, at the edges of the region in which pure first order Bragg scattering is expected to dominate. When significant energy resides in the tilting waves then the results will be affected by specular reflection at one extreme and grazing effects at the other. Our efforts here are primarily directed at the Bragg scattering cross-sections so that the model can be expected to perform best at mean incidence angles from 30° to 50°.

Figures 5 and 6 illustrate the models ability to track observed upwind/crosswind and upwind/downwind differences. While there is considerable scatter the standard deviation of points from the 45^o line in figure 5 is still only 1·46 dB.

In Figure 6 the data at all but the smallest angles ($\sim 19^o$) show reasonable agreement between model and observations. At 19^o the observations are consistently negative (i.e. downwind greater than upwind) while the model values, though relatively small, are always positive.

To complete the comparison of model and observed σ^o_{vv} we show (Figure 7) the entire-azimuth variation for three examples. This flight was chosen because the fit (22) at 40.8° incidence had a high correlation (0.91) and agreement with the model at up, down and crosswind was good. The point here is to illustrate the shape of the model's azimuth behaviour compared to that observed. Evidently, the characteristic shape of the observations is closely modelled.

As remarked earlier the σ^o_{HH} values are less easily modelled and this is illustrated in Figure 8. The observed and calculated $\sigma^o_{vv}/\sigma^o_{HH}$ ratios are well correlated but the calculated values are consistently high particularly at high incidence angles. Evidently some additional effect at horizontal polarization not contained in the model, is augmenting the observed σ^o_{HH} values. Recently Alpers (1984) has demonstrated the importance of "wedge scattering" to σ^o_{HH} particularly at high incidence angles. Generally it would appear that σ^o_{vv} is a more reliable indicator of wind effects on the ocean.

The RADSCAT data of Schroeder et al (1984) has served us well in tuning and testing the model. However, all of these data were obtained at the single frequency of 13·9 GHz and it would be wise to test the model at other microwave frequencies. Such data have been obtained by Valenzuela et al (1971) at four microwave frequencies from 0·4 to 8.9 GHz (P-band to X-band) and various incidence angles. They inverted a composite model to deduce the wave-number spectra over wave numbers from 0.09 to 3.5 cm^{-1}. Their spectra (actually from Valenzuela's, 1978 replot), which were obtained with the radar looking upwind, (i.e. Ψ (k,0)) are reproduced in Figure 9. They included 8 runs with wind speeds in the range of 2.5 to 24 m/s. Since we would like to examine the wave number dependence at constant wind we have omitted 2 of their cases - those with winds between 10 and 15 m/s. The other six cases correspond to: (a) one case of very light (2·3 m/s) winds; (b) five cases of moderate winds with mean of 18·3 m/s and standard deviation of 2·2 m/s. The wind speeds were obtained from ships, and have been adjusted to 10 m. It is clear that the spectrum varies in slope from less than k^{-4} at wavenumbers less than 1 to greater than k^{-4} at higher wavenumbers. The spectrum (9) is also shown and exhibits the same trend and is in close agreement with the observations above wavenumbers of 0.25 cm^{-1} i.e. wave lengths less than 25 cm.

The model results are also indicated for wind speeds of 2·4 m/s and 3·0 m/s. The model output for U_{10} = 3·0 m/s is in good agreement with the observations at 2·4 m/s. At these very low wind speeds ship anemometers would be operating near their thresholds and, during lulls, may stop thereby underestimating the mean wind.

Comments and qualifications

A typical RADSCAT circle flight experiment required several hours before all the data could be collected. The winds tabulated by Schroeder et al. (1984) are given to the nearest 0.1 m/s. However, they are based on wind speed averages for times much shorter than the circle flights. The reported winds may be considerably different from the most representative neutral stability wind to be used to fit the circle flight data (Pierson, 1983). It is not at all improbable that the reported winds could be in error by several meters per second. The total data set shows a number of circle flights for the same incidence angle wherein the backscatter for a higher reported wind is less than that for a lower wind. The scatter in Figure 4 may be, in part, the result of poor wind data. The 19.5 metre winds reported by Schroeder, et al. (1984) have had the effects of stability removed by means of the Monin-Obukhov (1954) theory and refer to neutral stability winds. The equations were closed by a relationship between z_0 and u_* given by Cardone (1969), with possible modifications. Such corrections have little effect on $U_{19.5}$ when different closures are used (i.e. Garrett (1977) versus Cardone (1969)) but can result in substantial differences in the wind stress and in the variation of wind with height close to the sea surface. Rather striking evidence for this appeared in a recent paper by Keller et al. (1984) in which the dependence of X-band backscatter on wind speed and atmospheric stability was investigated. The wind speed measurements were made at a height of 24.7 m and the relative backscattering cross-section, from tower measurements, showed a strong dependence on wind speed (their Figure 7). The scatter about the curve (wind speed to the power 2.3) shown is clearly related to atmospheric stability, with the cross section for the most unstable data almost a factor of three above the curve. The stability dependence is more clearly illustrated in their Figure 8. As explained earlier, these stability effects arise because the wind speed is measured at considerable height and the wind input term (5) is related to the wind very near the surface (for X-band at 45° incidence, $\lambda/2 = 1.13$ cm).

The ocean surface temperature that was used to compute the viscosity is the average of the temperatures of the data in Table I. The use of actual temperatures for each run could improve the fit. The reported temperatures varied from 8.5 °C to 17.9°C. The mean was 13.4°C and the standard deviation was 3.4°C.

Future programs to determine the ultimate accuracy of remotely sensed winds will require far more accurate conventionally measured winds averaged over an adequate time interval and better information on the sea surface temperature.

Wind range of scatterometry

The model has been quite successful in tracking the observations in a moderate range of wind speeds 5·5 m/s to 20 m/s. It is interesting to explore the models performance over wider wind speed ranges, particularly the high end associated with intense storms. In figures 10, 11 and 12 we have graphed σ^o_{vv} versus $U_{19.5}$ on (decibel) logarithmic scales from 1 m/s to 100 m/s for 3 radar wavenumbers and 3 incidence angles. The radar

wavenumbers chosen are those used by Seasat-SASS (3.06 cm^{-1}), the Seasat-SAR (0.267 cm^{-1}) and that planned for the European Research Satellite ERS-1 (1.11 cm^{-1}). According to the model the useful wind speed range of scatterometry is limited at the low end by viscosity for short waves and by the rapid diminution of the wind input term for the longer faster waves. On the other hand, the high wind speed end is limited too and the limit occurs sooner the shorter the Bragg wavelength. Here the cut off occurs because as the wind speed increases so does the prescribed drag coefficient. Thus the wind gradient increases and, although the wind at 19.5 m increases, the wind near the crest of the short waves actually decreases. Observations of σ^o_{vv} versus wind speed show a tendency to saturate at about 20 m/s at low incidence angles. See, for example, Woiceshyn et al. (1984a) and Jones et al. (1982), Figure 14. However, such data should be sorted by incidence angle to reveal these effects more clearly.

Figures 10 to 12 also illustrate the effect of water viscosity on the low wind speed response. For the highest wavenumber (Figure 10) there is a pronounced difference for water viscosity corresponding to tropical temperatures (20°C) from that for higher latitudes (0°C). Clearly scatterometers will report higher mean winds in the tropics than at high latitudes under light wind conditions if these corrections are not made.

A comparison of Figs. 10, 11 and 12 yields many interesting features. For K_u band, an approximate power law relationship for 20°C water extends from 4 m/s to 12 m/s at 25° incidence angle. The effect of temperature, which determines viscosity, is evident below 10 m/s and results in a 30 db drop between 2.5 and 3.5 m/s. For the higher incidence angles an approximately linear power law fails below 7 m/s. The most dramatic effects of temperature occur below winds of 7 m/s. The backscatter versus

wind speed relationship is monotonically increasing and not too sharply curved up to about 35 and 40 m/s at 45° and 65° respectively. At 16 m/s, backscatter varies from -3.5 to -19.5 db as the incidence angle varies from 25° to 65°.

For a fixed temperature and incidence angle the curves are monotonically increasing over a considerable range of wind speeds. For a scatterometer, the σ^0 (V, χ, θ, T) function will be known uniquely as a function of V and χ and consequently, SEASAT-like measurements and future systems will be able to recover vector winds. For hurricanes and low incidence angles some care in interpretation will be needed.

At the inner edge of a scatterometer swath, for cold water, winds below 3 m/s may be unmeasurable. At the outer edge, winds below 5 m/s may be unmeasurable. These double logarithmic scales need to be studied very carefully, especially since the errors in conventional anemometry are not related to the logarithm of the wind speed.

For K_u band, the large range in the different power laws that various investigators have found can be seen now to be a function of water temperature and the actual sample of wind speeds versus backscatter plus the curve fitting methods. Straight lines through such clouds of points can have wide variations in slope.

Figure 10 illustrates the basic difficulty of trying to fit a power law to backscatter versus wind speed data. For example, at 25° incidence angle the two curves shown for 0°C and 20°C (water temperature) are more or less straight from 6 or 7 m/s to 15 or 16 m/s. However, depending on water temperature, they fall off to undetectable values between 6 and 3 m/s. At higher wind speeds the curves merge and finally roll over at some maximum near 22 m/s. A power law fitted to data from randomly selected wind speeds over this range can be more or less steep than the straight portion depending on the relative abundance of data under 6 m/s and above 17 m/s.

For the three incidence angles plotted there will be additional difficulties at light winds because of variations in the sea surface temperature (Woiceshyn et al. 1984b).

For C band, the range for an approximately linear power law extends from 4 m/s to nearly 26 m/s, 50 m/s and 63 m/s for 20° C water and incidence angles of 25°, 45° and 65° respectively. The backscatter at 16 m/s varies from -5.5 db to -16 db from 25° to 65° incidence angle. If the variance of the estimate of the backscatter can be kept very low, C band may prove to be the best design frequency for a scatterometer. Problems associated with attenuation by large water drops in clouds and by rain would be minimized.

For L band, an even wider range of wind speeds is covered by an almost straight curve. Viscosity is much less important. Since the wave number is a factor of 10 smaller than at K_u band, further study is needed because the present results were tuned at K_u band. At 16 m/s the backscatter varies from -10 db to -19.5 db.

It should be noted that the model calculations presented in Figures 10, 11 and 12 cover a much wider range of wind speeds than the circle flight data (Schroeder et al., 1984) used to verify this model. Thus the predicted roll-off of backscatter at high wind speeds and the viscosity dependent low wind speed cut-off should be verified against other data when such are available.

We further remark that the wind speed dependence predicted by the model is dependent on the choice of α and n in equation (9). As we remarked earlier, it is unlikely that α and n will have the same values for purely gravity waves as they do for the capillary-gravity waves for which the model was tuned. In particular, we expect n to be larger for gravity waves than for capillary waves, so that it is likely that the true wind speed dependence of L band (and to lesser extent, C band) will be weaker than that depicted in Figure 12.

Acknowledgements

One of the authors (M.A.Donelan) was a guest of the Max-Planck-Institut für Meteorologie, Hamburg, and the recipient of a research fellowship from the Alexander von Humboldt Stiftung, Bonn, during the course of this work. He wishes to thank both these organizations for their hospitality and generosity.

The contribution of W.J. Pierson to this research was supported under NASA contract number NAGW-266.

References

Alpers. W. (1984): Personal Communication.

Al-Zanaidi, M.A. and W.H. Hui (1984): Turbulent air flow over water waves - a numerical study (in press) J. Fluid Mech.

Barrick, D.E. and W.H. Peake (1968): A review of scattering from surfaces with different roughness scales. Radio Sci. 3, pp. 865-868.

Brown, R.A. (1983): On a satellite scatterometer as an anemometer. SEASAT II. Scientific Results. J. Geophys. Res. 88, No. C3. pp 1663 - 1673.

Cardone, V.J. (1969): Specification of the wind field distribution in the marine boundary layer for wave forecasting. Rep. JR-69-1, Geophysics Science Lab., New York Univ.

Chan, H.L. and A.K. Fung (1977): A Theory of Sea Scatter at Large Incident Angles. J. Geophys. Res. 82, No. 24. pp 3439 - 3444.

Chia, R.C. (1968): The theory of radar backscatter from the sea. PH.D. Thesis Univ. of Kansas. 120 pp.

Cox, C.S. (1958): Measurements of slopes of high-frequency wind waves. J. Marine Res. 16, pp. 199-225.

Cox, C. and W. Munk (1954): Statistics of the sea surface derived from sun glitter. J. Marine Res. 13, pp. 198-227.

Crapper, G.D. (1957): An exact solution for progressive capillary waves of finite amplitude. J. Fluid Mech. 2, No. 6, pp 532 - 540.

Donelan, M.A. (1982): The dependence of the aerodynamic drag coefficient on wave parameters. First Internat. Conference on Meteorology and Air Sea Interaction of the Coastal Zone. pp 381 - 387. Amer. Meter. Soc. Boston, Mass.

Donelan, M.A., J. Hamilton and W.H. Hui (1984): Directional spectra of wind generated waves. Phil. Trans. Roy. Soc. (in press).

Donelan, M.A. and Pierson, W.J. (1984): Does the scatterometer see wind speed or friction velocity? Proc. Int. Union Radio Sci. Meeting, May 14 - 23, Shoresh, Israel. NASA Conference publication 2303.

Garrett, J.R (1977): Review of drag coefficients over oceans and continents, Mon. Wea. Rev., 105, pp 915 - 929.

Guinard, N.W., J.T. Ransone Jr. and J.C. Daley (1971): Variation of the NRCS of the sea with increasing roughness. J. Geophys. Res. 76, pp. 1525-1538.

Hasselmann, D., J. Bösenberg, M. Dunckel, K. Richter, M. Grünewald and H. Carlson (1983): Measurements of wave induced pressure over surface gravity waves. Proc. Internat. Union Radio Sci. Meeting, May 1981 Miami, USA.

Hsiao, S.V. and O.H. Shemdin (1983): Measurements of wind velocity and pressure with a wave follower during MARSEN. J. Geophys. Res. 88 No C 14, pp 9841 - 9849.

Jeffreys, H. (1924): On the formation of waves by wind. Proc. Roy. Soc. A, 107, pp. 189 - 206.

Jeffreys, H. (1925): On the formation of waves by wind. II. Proc. Roy. Soc. A. 110, pp. 341 - 347.

Jones, W.L., L.C. Schroeder and J.L. Mitchell (1977): Aircraft measurements of the microwave scattering signature of the ocean, IEEE J. Oceanic. Eng. OE-2, No. 1. pp 52 - 61.

Jones, W.L. and L.C. Schroeder (1978): Radar backscatter from the ocean: Dependence on surface friction velocity. Boundary Layer Meteor. 13, pp 133 - 149.

Jones, W.L., L.C. Schroeder, D.H. Boggs, E.M. Bracalente, R.A. Brown, G.J. Dome, W.J. Pierson and F.J. Wentz (1982): The SEASAT - A satellite scatterometer: the geophysical evaluation of remotely sensed wind vectors over the ocean. J. Geophys. Res., 87, pp 3297 - 3317.

Keller, W.C., W.J. Plant and D.E. Weissman (1984): The dependence of X-band microwave sea return on atmospheric stability and sea state. J. Geophys. Res. (in press).

Keller, W.C. and J.W. Wright (1975): Microwave scattering and the straining of wind-generated waves. Radio Sci. 10, pp. 139-147.

Kitaigorodskii, S.A. (1983) On the theory of the equilibrium range in the spectrum of wind generated gravity waves. J. Phys. Ocean. 13, pp 816 - 827.

Kitaigorodskii, S.A. and Yu A. Volkov (1965): On the roughness parameter of the sea surface and the calculation of momentum flux in the near water layer of the atmosphere. IZV, Atm. Ocean. Phys 1. pp 973 - 988.

Kondo, J. (1975): Air-sea bulk transfer coefficients in diabatic conditions. Bound.-Layer Meteor., 9, pp 91 - 112

Kondo, J., Y. Fujinawa and G. Naito (1983): High-frequency components of ocean waves and their relation to the aerodynamic roughness. J. Phys. Ocean., 3, pp 197 - 202.

Large, W.G. and S. Pond (1981): Open ocean momentum flux measurements in moderate to strong winds. J. Phys. Oceanogr. 11, pp 324 - 336.

Larson, T.R. and J.W. Wright (1975): Wind-generated gravity - capillary waves: Laboratory measurements of temporal growth rates using microwave backscatter. J. Fluid Mech., 70, pp. 417 - 436.

Liu, W.T. and W.G. Large (1981): Determination of surface stress by SEASAT-SASS. J. Phys. Oceanogr. 11, pp 1603 - 1611.

Longuet-Higgins, M.S. (1982): On the skewness of sea-surface slopes. J. Phys. Oceanogr. 12, pp. 1283-1291.

Michell, J.H. (1893): The highest waves in water. Phil. Mag. (5), 36, pp. 430 - 437.

Miles, J.W. (1957): On the generation of surface waves by shear flows. J. Fluid Mech. 3, pp. 185 - 204.

Miles, J.W. (1959): On the generation of surface waves by shear flows. Part 2. J. Fluid Mech. 6 pp. 568 - 582.

Mitsuyasu, H. and T. Honda (1975): The high frequency spectrum of wind-generated waves. Rep. Res. Inst. Appl. Mech. Kyushu University, 22, pp. 327-355.

Monin, A.S. and A.M. Obukhov (1954): Basic laws of turbulent mixing in the ground layer of the atmosphere. Akademiia Nauk SSSR Leningrad. Geofizicheskii, Institut Trudy No. 24 (151) pp 163 - 187.

Moore, R.K. and A.K. Fung, (1979): Radar determination of winds at sea. Proc. of IEEE,. 67, pp 1504 - 1521.

Phillips, O.M. (1958): The equilibrium range in the spectrum of wind generated waves. J. Fluid Mech. 4. pp 426 - 434.

Pierson, W.J. (1983): The measurement of the synoptic scale wind over the ocean. J. Geophys. Res. 88, C3, pp 1683 - 1708.

Pierson, W.J. and Salfi, R.E. (1982): Monte Carlo studies of ocean wind vector measurements by SCATT: Objective criteria and maximum likelihood estimates for removal of aliases, and effects of cell size on accuracy of vector winds. NASA Contractor Report 165837 - 1 Langley Research Center, Hampton Virginia 23665.

Pierson, W.J. and R.A. Stacy (1973): The elevation slope, and curvature spectra of a wind roughened sea surface. NASA Contractor Rep. CR-2646.

Plant, W.J. (1982): A relationship between wind stress and wave slope. J. Geophys. Res. 87, No. C3 pp. 1961 - 1967.

Reece, A.M. Jr., (1978): Modulation of short waves by long waves. Boundary Layer Meteor. 13, pp 203 - 214.

Rice, S.O. (1951): Reflection of electromagnetic waves from slightly rough surfaces, Comm. Pure Appl. Math. 4, Mos 2/3. pp 361 - 378.

Schlichting, J. (1968): Boundary Layer Theory, 6th ed. Mc Graw-Hill. 747 pp.

Schooley, A.H. (1958): Profiles of wind-created water waves in the capillary-gravity transition region. J. Marine Res. 16, pp. 100-108.

Schroeder, L.C., W.L. Grantham, J.L. Mitchell and J.L. Sweet (1982a): SASS measurements of the K_u-band radar signature of the ocean. IEEE J. Oceanic Eng., OE-7, pp 3 -14.

Schroeder, L.C., D.H. Boggs, G.J. Dome, I.M. Halberstam, W.L. Jones, W.J. Pierson and F.J. Wentz (1982b): The relationship between wind vector and normalized radar cross section used to derive SEASAT-A satellite scatterometer winds. J. Geophys. Res., 87, pp 3318 - 3336.

Schroeder, L.C., W.L. Jones, P.R. Schaffner and J.L. Mitchell (1984). Flight measurement and analysis of AAFE RADSCAT wind speed signature of the ocean. NASA Tech. Memorandum 85646, 144 pp.

Smith, S.D. (1974): Eddy flux Measurements over Lake Ontario, Bdy. Layer Meteor. 6, pp 235 - 255.

Smith, S.D. (1980): Wind stress and heat flux over the ocean in gale force winds. J. Phys. Ocean. 10 pp. 709 - 726.

Snyder, R.L., F.W. Dobson, J.A. Elliott and R.B. Long (1981). Array measurements of atmospheric pressure fluctuations above surface gravity waves. J. Fluid Mech., 102 pp 1 - 59.

Valenzuela, G.R. (1968): Scattering of electromagnetic waves from a tilted slightly rough surface. Radio Science, 3, pp 1057 - 1066.

Valenzuela, G.R. (1976): The growth of gravity - capillary waves in a coupled shear flow. J. Fluid Mech. 76, pp. 229 - 250.

Valenzuela, G.R. (1978): Theories for the interaction of electromagnetic and oceanic waves - a review. Bdy. Layer Meteor. 13, pp. 61-85.

Valenzuela, G.R., M.B. Laing and J.C. Daley (1971): Ocean spectra for the high-frequency waves as determined from airborne radar measurements. J. Marine Res., 29, pp 69 - 84.

Weast, R.C. (1970). Handbook of Chemistry and Physics, 50th Edition, The Chemical Rubbber Company.

Woiceshyn, P.M., M.G. Wurtele, D.H. Boggs, L.F. McGoldrick and S. Peteherych (1984a). A new parameterization of an empirical model for wind/ocean scatterometry. Proc. Internat. Union Radio Sci. Meeting, May 14-23, Shoresh, Israel. NASA Coference Publication 2303.

Woiceshyn, P.M., M.G. Wurtele, D.H. Boggs and L.F. McGoldrick (1984b). The relationship of scatterometer radar return from the ocean surface to wind, wind stress and other geophysical parameters. (In preparation).

Wright, J.W. (1966): Backscattering from capillary waves with application to sea clutter. IEEE Trans. on Ant. and Prop., AP-14, pp 749-- 754.

Wright, J.W. (1968): A new model for sea clutter. IEEE Trans. on Ant. and Prop., AP-16, pp 217 - 223.

Wright, J.W. and W.C. Keller (1971): Doppler spectra in microwave scattering from wind waves. Physics of Fluids, 14, pp. 466-474.

Yaplee, B.S., A. Shapiro, B.D. Hammond and E.A. Uliana (1971): Nanosecond radar observations of the ocean surface from a stable platform. IEEE Trans. GE-9, pp. 170-174.

TABLE I.

Summary of the Best Circle Flight Data From Schroeder et al. 1984

Flt. No.	Line/ Run	$\bar{\theta}$	$\bar{U}_{19.5}$ m/s	σ^o_{vv} A_0 x10^3	A_1 x10^3	A_2 x10^3	R^2	σ^o_{vv} (dB) Up	Down	Cross	$\bar{U}_{19.5}$ (dB)	σ^o_{vv} up/cross (dB)	σ^o_{vv} up/down (dB)	σ^o_{HH} A_0 x10^3	A_1 x10^3	A_2 x10^3	R^2	σ^o_{HH} (dB) Up	Down	Cross	$\sigma^o_{vv}/\sigma^o_{HH}$ (dB) Up	Down	Cross
318/14	4/7	39.9	5.5	3.967	0.808	1.799	.762	-21.82	-23.05	-26.64	7.40	4.82	1.23	2.024	0.996	0.819	.865	-24.16	-27.34	-29.19	2.34	4.29	2.55
	12	67.2	5.5	0.783	0.081	0.416	.874	-28.93	-29.52	-34.35	7.40	5.42	0.59	0.145	0.061	0.026	.473	-36.35	-39.59	-39.24	7.42	10.07	4.89
16	4/9	39.4	8.2	9.153	1.497	5.648	.732	-17.88	-18.76	-24.55	9.14	6.67	0.88	5.04	2.23	2.599	.739	-20.06	-22.67	-26.12	2.18	3.91	1.57
	14	66.2	8.9	2.869	0.161	2.228	.851	-22.79	-23.07	-31.93	9.49	9.14	0.28	0.267	0.154	0.163	.762	-32.34	-35.59	-39.83	9.55	12.52	7.90
17	4/1	19.8	13.5	516.6	-51.61	148.5	.811	-2.12	-1.45	-4.34	11.30	2.22	-0.67	555.5	-30.38	143.4	.688	-1.75	-1.37	-3.85	-0.37	-.08	-.49
	8	40.8	12.8	25.7	3.977	15.42	.911	-13.46	-14.30	-19.88	11.07	6.42	0.84	14.10	5.258	7.611	.898	-15.69	-17.84	-21.88	2.23	3.54	2.0
	12	68.1	12.3	6.311	1.512	3.752	.913	-19.36	-20.68	-25.92	10.90	6.56	1.32	0.977	0.681	0.462	.914	-26.74	-31.20	-32.88	7.38	10.52	6.96
18	4/6	40.4	11.3	17.51	4.634	12.67	.877	-14.58	-15.93	-23.15	10.53	8.57	1.35	9.409	3.865	4.439	.822	-17.52	-20.01	-23.04	2.94	4.08	-0.11
	11	65.5	10.5	6.67	0.458	4.838	.935	-19.22	-19.57	-27.37	10.21	8.15	0.35	1.07	0.376	0.657	.917	-26.77	-28.69	-33.84	7.55	9.12	6.47
19	4/13	40.9	7.5	10.47	0.927	6.394	.879	-17.50	-17.98	-23.90	8.75	6.40	0.48	5.182	1.858	2.555	.834	-20.18	-22.31	-25.81	2.68	4.33	1.91
	17	67.1	7.5	2.573	0.389	2.034	.893	-23.01	-23.75	-32.68	8.75	9.67	0.74					Data Missing					
24	4/1	30.3	9.5	59.14	10.21	25.29	.815	-10.24	-11.29	-14.70	9.78	4.46	1.05	38.63	8.093	12.84	.745	-12.25	-13.63	-15.89	2.01	2.34	1.19
335/4A	4/1	18.9	19.8	833.6	-29.74	321.0	.807	+.511	+.735	-2.902	12.97	3.41	-0.22	844.4	-0.613	319.7	.797	+.658	+.662	-2.80	-.147	+.073	-0.102
	9	39.1	20.0	55.18	0.113	26.67	.760	-10.86	-10.88	-15.45	13.01	4.59	0.02	31.70	2.33	15.93	.737	-13.01	-13.44	-18.02	2.15	2.56	2.57
	17	58.2	19.8	15.09	4.643	5.175	.753	-16.04	-18.06	-20.04	12.97	4.00	2.02	4.43	2.301	1.409	.706	-20.89	-24.51	-25.20	4.85	6.45	5.16
4B	4/1	19.0	19.1	802.7	-94.86	247.6	.539	-0.198	+0.589	-2.56	12.81	2.36	-0.79	815.8	-40.67	259.0	.571	+.146	+.475	-2.54	-.344	+.114	-.02
	10	38.7	19.4	69.39	14.97	27.17	.710	-9.53	-10.88	-13.74	12.88	4.21	1.35	44.81	14.64	16.63	.703	-11.19	-13.30	-15.50	1.66	2.42	1.76
5	4/1	19.9	15.5	632.9	-8.396	235.5	.655	-0.655	-0.571	-4.008	11.90	3.35	-0.08	640.6	10.74	235.4	.642	-.522	-.629	-3.92	-.133	+.058	-.088
	9	39.4	15.2	39.52	5.693	18.55	.706	-11.95	-12.81	-16.78	11.82	4.83	0.86	22.82	7.03	10.29	.699	-13.96	-15.84	-19.02	2.01	3.03	2.24
	17	58.5	15.1	12.58	3.103	5.132	.789	-16.82	-18.35	-21.28	11.79	4.46	1.53	3.013	1.678	1.410	.684	-22.15	-25.61	-27.95	5.33	7.26	6.67
6	4/9	39.1	15.0	37.74	6.541	17.45	.748	-12.09	-13.13	-16.93	11.76	4.84	1.04	20.48	6.94	8.62	.728	-14.43	-16.54	-19.26	2.34	3.41	2.33
	13	57.8	15.0	12.53	3.169	5.31	.857	-16.78	-18.34	-21.41	11.76	4.63	1.56	3.002	1.495	1.246	.800	-22.41	-25.60	-27.55	5.63	7.26	6.14
353/11	4/1	67.3	16.0	8.617	2.834	4.337	.825	-18.02	-19.95	-23.69	12.04	5.67	1.93	1.443	1.095	.806	.779	-24.76	-29.38	-31.96	6.74	9.43	8.27
	11	39.7	15.7	41.95	7.256	19.10	.792	-11.66	-12.69	-16.41	11.96	4.75	1.03	22.82	7.872	9.771	.700	-13.93	-16.07	-18.84	2.27	3.38	2.43

TABLE II

Model Calculations Corresponding to the Data in Table I

Flt. No.	Line/ Run	$\bar{\theta}$	$\bar{U}_{19.5}$ m/s	σ^o_{vv} (dB)			σ^o_{vv} up/cross (dB)	σ^o_{vv} up/down (dB)	$\bar{U}_{19.5}$ (dB)	σ^o_{HH} (dB)			$\sigma^o_{vv}/\sigma^o_{HH}$ (dB)		
				Up	Down	Cross				Up	Down	Cross	Up	Down	Cross
318/14	4/7	39.9	5.5	-20.25	-20.41	-28.34	8.09	0.16	7.40	-26.19	-26.48	-34.38	5.95	6.07	6.04
	12	67.2	5.5	-29.83	-30.12	-38.09	8.26	0.29	7.40	-45.66	-46.20	-54.17	15.83	16.08	16.07
16	4/9	39.4	8.2	-16.66	-17.07	-23.41	6.75	0.41	9.14	-21.74	-22.44	-28.56	5.08	5.37	5.15
	14	66.2	8.9	-23.43	-24.06	-31.75	8.32	0.63	9.49	-36.83	-38.03	-45.48	13.40	13.97	13.73
17	4/1	19.8	13.5	- 0.69	- 1.31	- 3.63	2.94	0.62	11.30	- 1.09	-1.76	- 3.88	0.40	0.44	0.25
	8	40.8	12.8	-13.89	-14.89	-19.63	5.74	1.00	11.07	-17.93	-19.53	-23.87	4.04	4.64	4.24
	12	68.1	12.3	-21.41	-22.55	-28.53	7.12	1.14	10.90	-33.52	-35.50	-41.04	12.11	12.95	12.51
18	4/6	40.4	11.3	-14.67	-15.45	-20.56	5.89	0.78	10.53	-19.06	-20.35	-25.13	4.40	4.90	4.57
	11	65.5	10.5	-21.98	-22.80	-29.51	7.53	0.82	10.21	-34.21	-35.73	-42.04	12.23	12.93	12.54
19	4/13	40.9	7.5	-17.88	-18.21	-25.22	7.34	0.33	8.75	-23.56	-24.15	-30.94	5.68	5.94	5.73
	17	67.1	7.5	-25.19	-25.67	-33.54	8.35	0.48	8.75	-39.80	-40.73	-48.53	14.62	15.06	14.99
24	4/1	30.3	9.5	-11.64	-12.26	-17.31	5.67	0.62	9.78	-14.28	-15.16	-20.02	2.64	2.90	2.71
335/4A	4/1	18.9	19.8	+ 0.01	- 0.56	- 1.71	1.72	0.57	12.97	- 0.27	- 0.89	- 1.77	0.28	0.34	0.07
	9	39.1	20.0	- 9.42	-11.54	-14.79	5.37	2.12	13.01	-11.33	-14.07	-16.74	1.91	2.53	1.95
	17	58.2	19.8	-16.17	-18.09	-22.31	6.14	1.92	12.97	-22.34	-25.40	-28.86	6.18	7.31	6.55
4B	4/1	19.0	19.1	- 0.14	- 0.66	- 1.71	1.57	0.52	12.81	- 0.43	- 1.00	- 1.78	0.29	0.34	0.07
	10	38.7	19.4	- 9.53	-11.56	-14.86	5.33	2.03	12.88	-11.48	-14.13	-16.85	1.96	2.57	1.99
5	4/1	19.9	15.5	- 0.23	- 0.86	-2.76	2.53	0.63	11.90	- 0.58	- 1.26	- 2.94	0.35	0.39	0.18
	9	39.4	15.2	-11.99	-13.39	-17.54	5.55	1.40	11.82	-15.03	-17.10	-20.78	3.04	3.71	3.24
	17	58.5	15.1	-17.94	-19.24	-24.23	6.29	1.30	11.79	-25.86	-28.13	-32.54	7.91	8.89	8.31
6	4/9	39.1	15.0	-11.97	-13.35	-17.52	5.55	1.38	11.76	-15.00	-17.04	-20.75	3.03	3.69	3.22
	13	57.8	15.0	-17.82	-19.10	-24.09	6.27	1.28	11.76	-25.58	-27.82	-32.23	7.75	8.72	8.14
353/11	4/1	67.3	16.0	-19.48	-21.09	-26.10	6.62	1.61	12.04	-29.53	-32.19	-36.60	10.05	11.10	10.51
	11	39.7	15.7	-11.85	-13.33	-17.40	5.55	1.48	11.96	-14.82	-16.99	-20.57	2.97	3.66	3.17

Figure Captions

1. Normalized exponential growth rates versus $U(\lambda/2)/c(\lambda) - 1$. The data are taken from Larson and Wright (1975) and the different symbols refer to different wave lengths of the growing water wave:

   0.72 cm (▲); 1.25 cm (+); 1.85 cm (Δ);

   2.72 cm (o); 4.05 cm (x); 6.98 cm (●)

   The dashed line corresponds to Eq. (5) and the solid line to Eq. (4).

2. Normalized exponential growth rates versus $u_*/c(\lambda)$. As in Fig. 1, the data are from Larson and Wright (1975). The line shown has a slope of 2.

3. Normalized exponential growth rates versus $U_{19.5}/c(\lambda)$. As in Fig. 1, the data are from Larson and Wright (1975). The line shown has a slope of 2.

4. Model calculations of σ^o_{vv} versus the circle flight observations of Schroeder et al. (1984). The line of perfect agreement is shown. The symbols correspond to different radar incidence angles: 19°(+); 30°(□); 40°(●); 58° (x); 67°(o).

5. Model calculations of the ratio of upwind to crosswind vv backscatter versus the observations of Schroeder et al. (1984). The line of perfect agreement is shown. The symbols correspond to different radar incidence angles: 19°(+); 30°(□); 40°(●); 58° (x); 67° (o).

6. Model calculations of the ratio of upwind to downwind vv backscatter versus the observations of Schroeder et al. (1984). The line of perfect agreement is shown. The symbols correspond to different radar incidence angles: 19°(+); 30°(□); 40°(●); 58° (x); 67°(o).

7. Comparison of the azimuth response of model with observations for 3 runs of Schroeder et al's (1984) flight 318/17. Model calculations for $\tilde{U}_{19.5}$ of 13.5 m/s (o) and 12.3 m/s (x); Shroeder et al's data (●).

8. Model calculations of the ratio of vv to HH backscatter versus the observations of Schroeder et al. (1984). The line of perfect agreement is shown. The symbols correspond to different radar incidence angles: 19°(+); 30°(□); 40°(•); 58° (x); 67°(o).

9. Calculated equilibrium wave spectra compared with the observations of Valenzuela et al. (1971).

10. Model calculations of expected K_u band backscatter for wind speeds in the range of 1 m/s to 100 m/s and for three incidence angles. The effect of surface water temperature (through viscosity) is also illustrated.

11. Model calculations of expected C band backscatter for wind speeds in the range of 1 m/s to 100 m/s and for three incidence angles. The effect of surface water temperature (through viscosity) is also illustrated.

12. Model calculations of expected L band backscatter for wind speeds in the range of 1 m/s to 100 m/s and for three incidence angles. The effect of surface water temperature (through viscosity) is also illustrated.

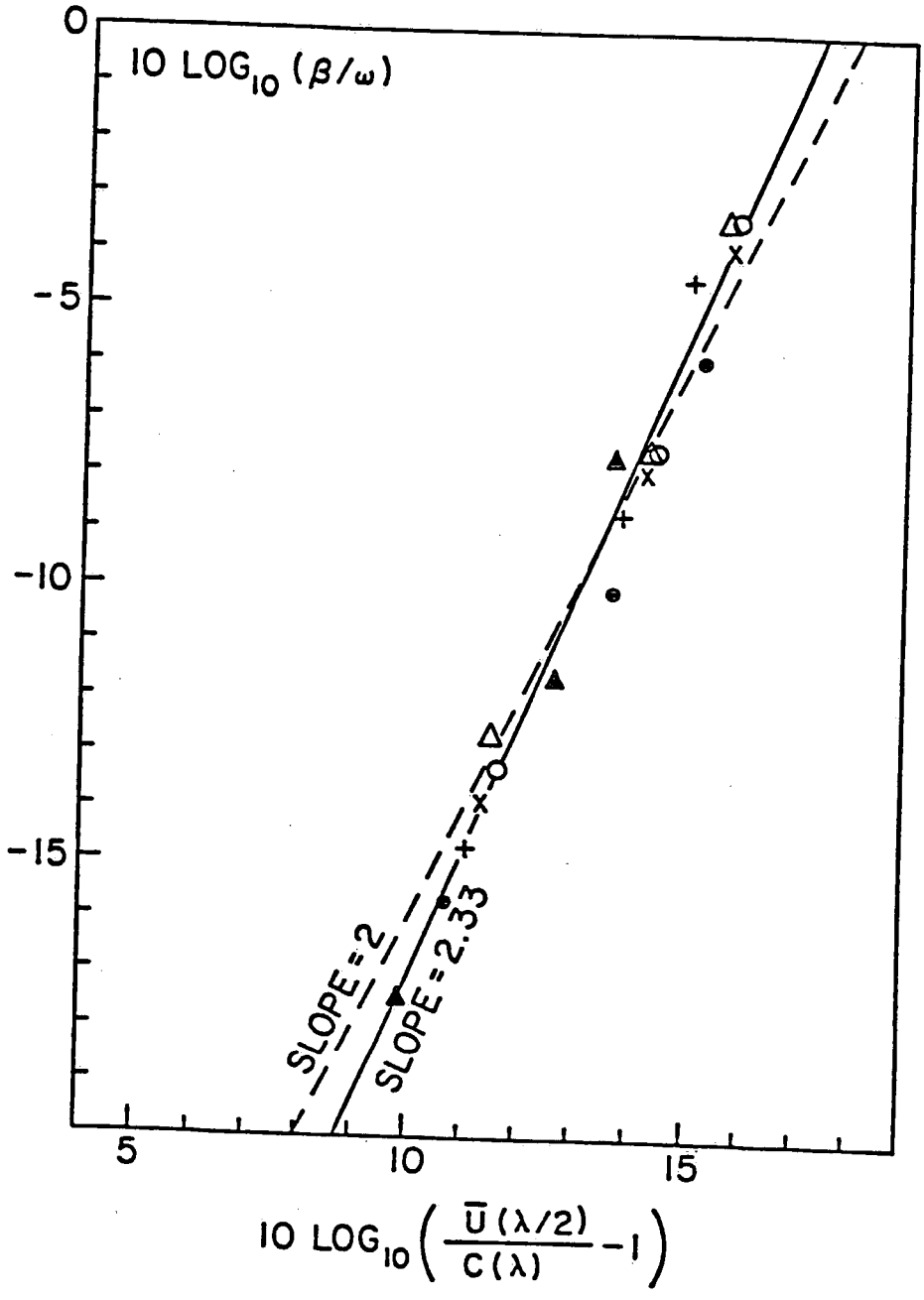

FIGURE 1.

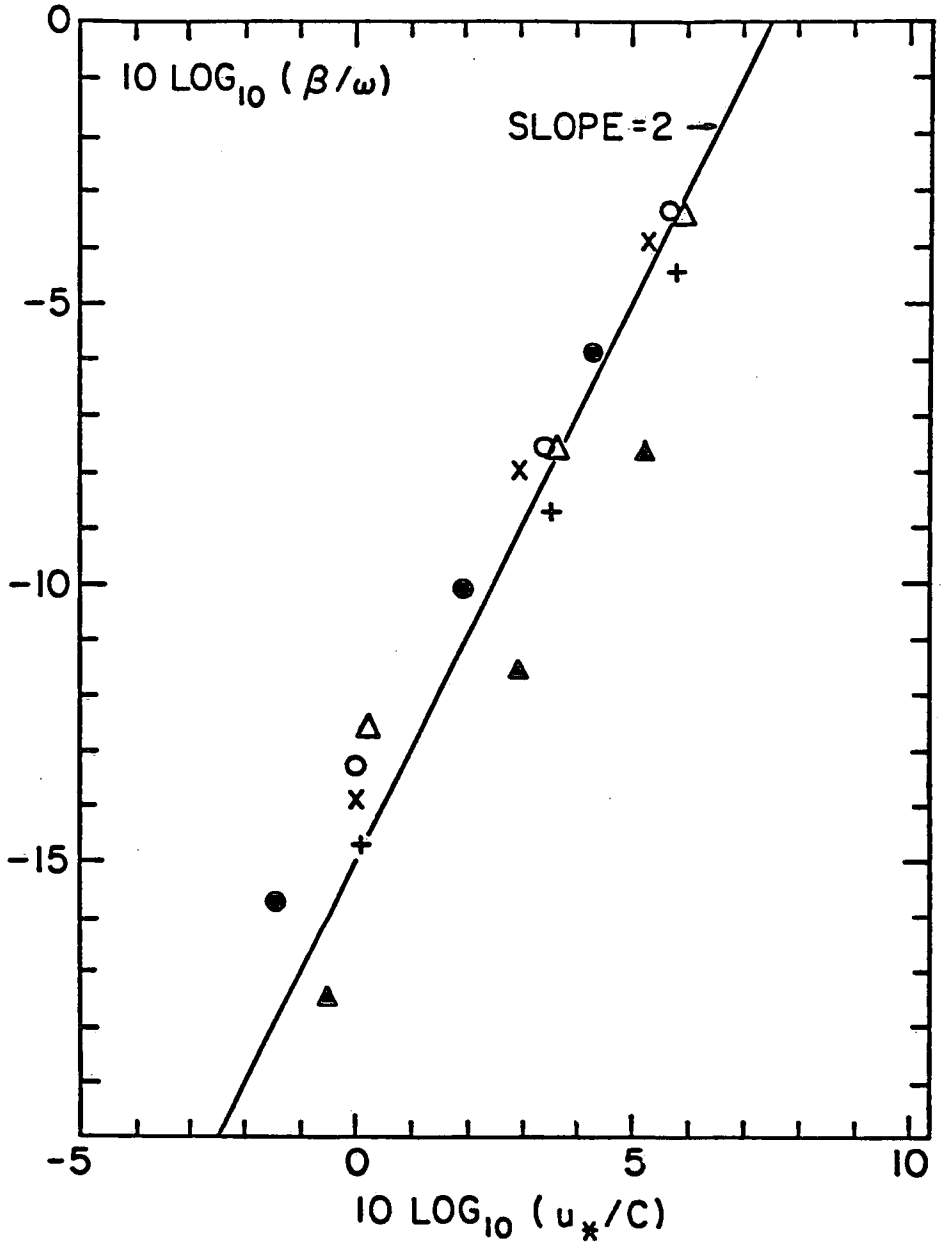

FIGURE 2.

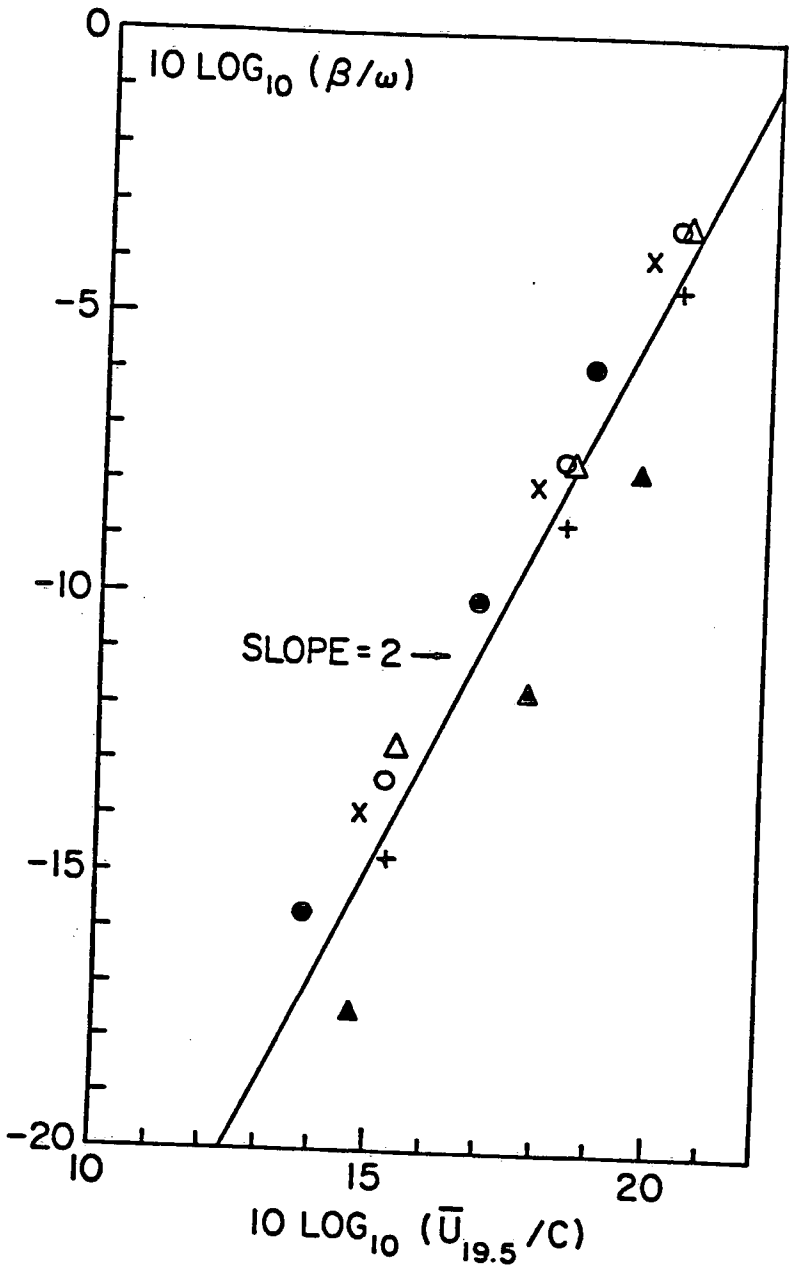

FIGURE 3.

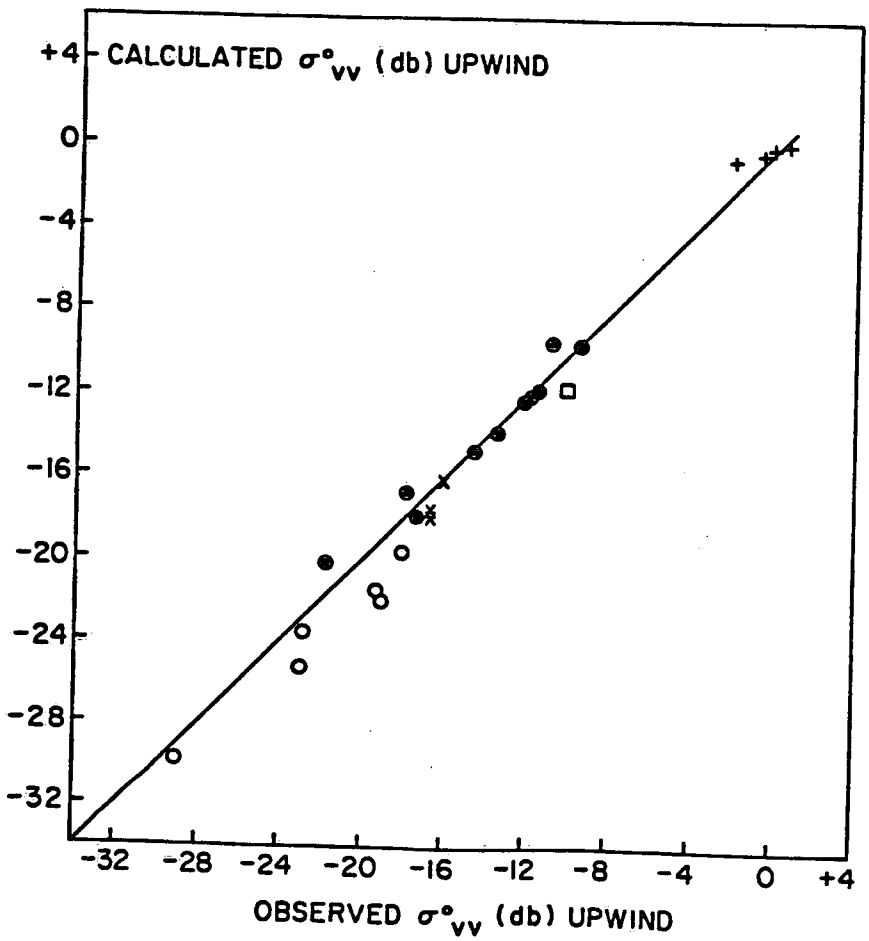
+4
0
-4
-8
-12
-16
-20
-24
-28
-32
CALCULATED σ°_{vv} (db) UPWIND
-32 -28 -24 -20 -16 -12 -8 -4 0 +4
OBSERVED σ°_{vv} (db) UPWIND

FIGURE 4.

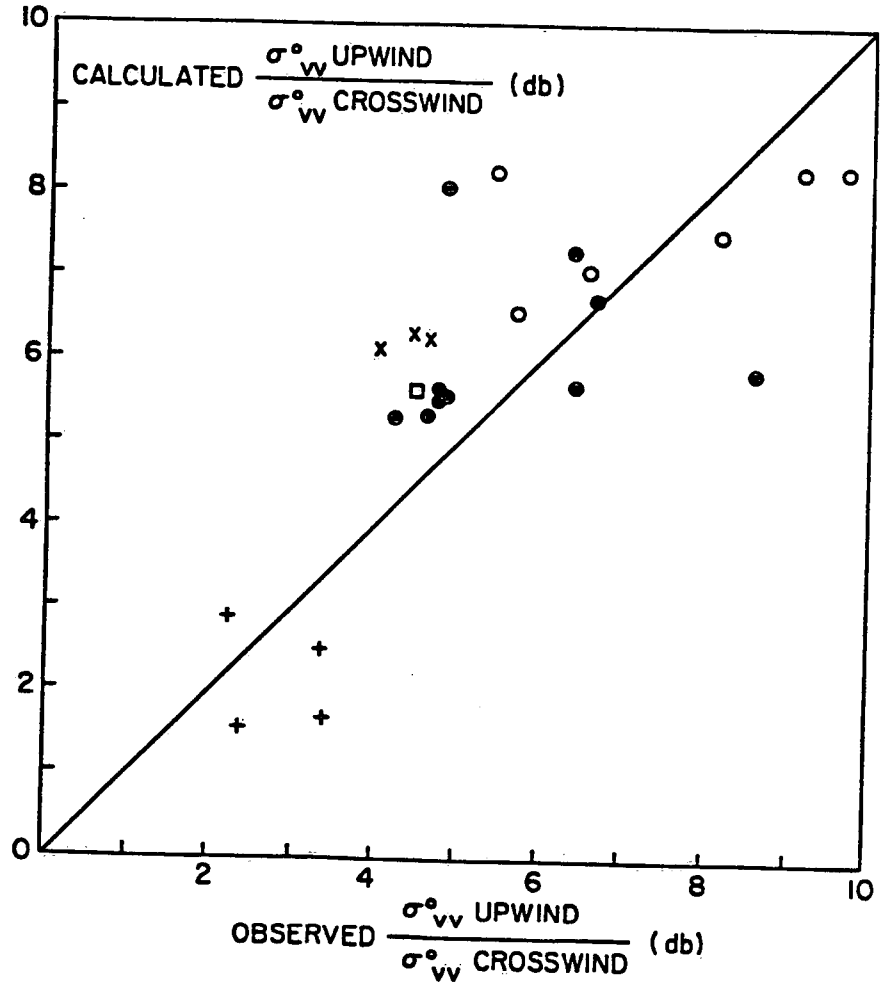
10
8
6
4
2
0
2
4
6
8
10
CALCULATED $\frac{\sigma^\circ_{vv}\ \text{UPWIND}}{\sigma^\circ_{vv}\ \text{CROSSWIND}}$ (db)
OBSERVED $\frac{\sigma^\circ_{vv}\ \text{UPWIND}}{\sigma^\circ_{vv}\ \text{CROSSWIND}}$ (db)

FIGURE 5.

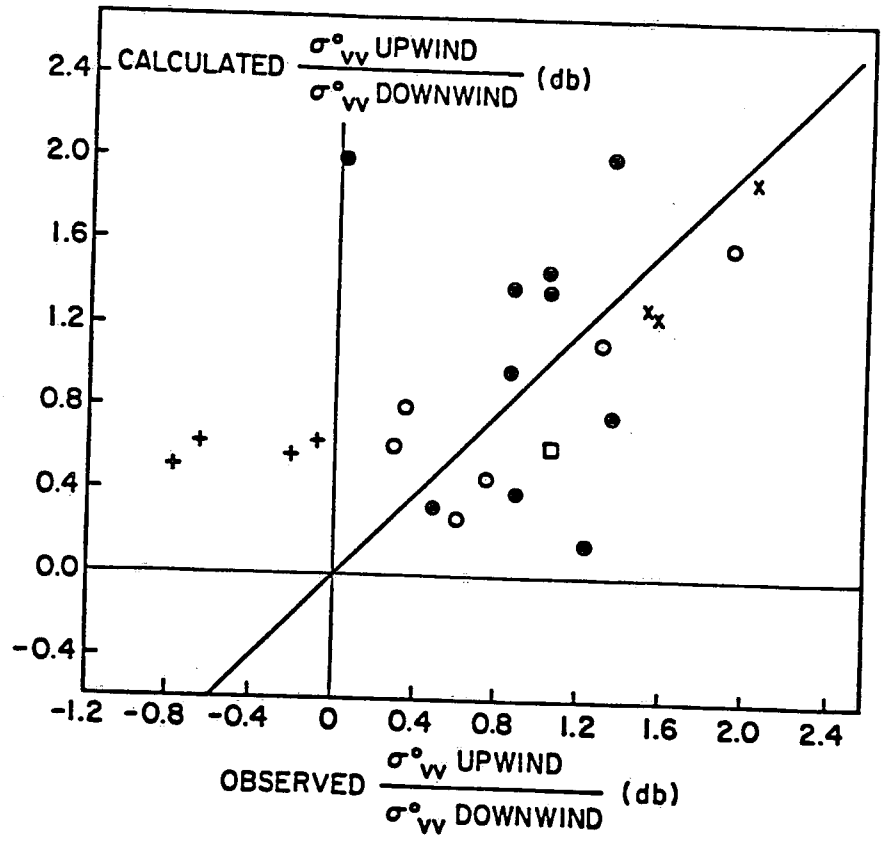
CALCULATED $\frac{\sigma^\circ_{vv}\ \text{UPWIND}}{\sigma^\circ_{vv}\ \text{DOWNWIND}}$ (db)
2.4
2.0
1.6
1.2
0.8
0.4
0.0
-0.4
-1.2 -0.8 -0.4 0 0.4 0.8 1.2 1.6 2.0 2.4
OBSERVED $\frac{\sigma^\circ_{vv}\ \text{UPWIND}}{\sigma^\circ_{vv}\ \text{DOWNWIND}}$ (db)

FIGURE 6.

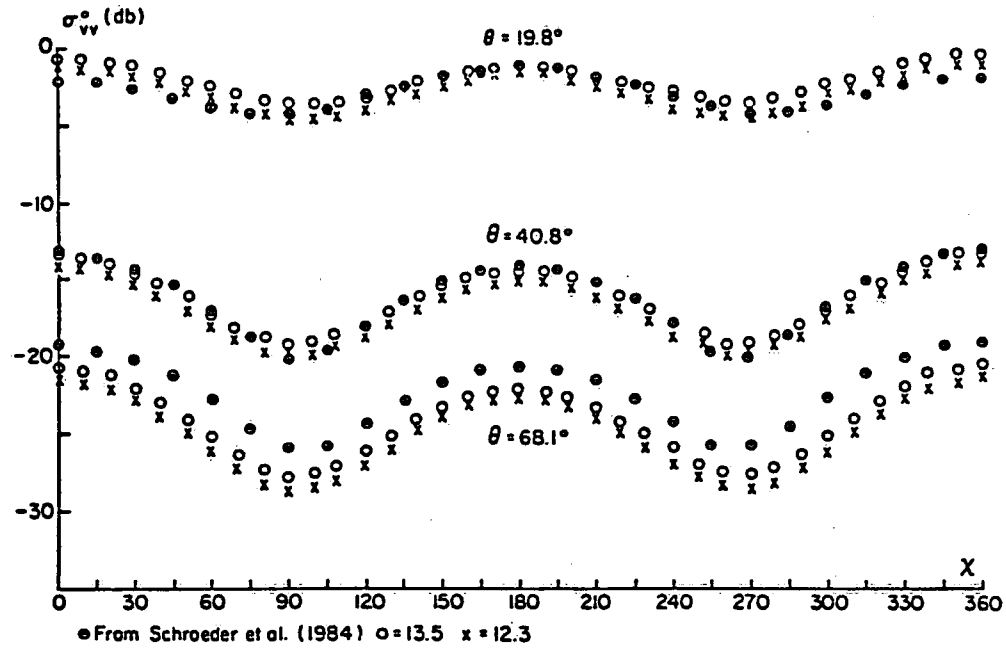
σ°_{vv} (db)
0
-10
-20
-30
θ = 19.8°
θ = 40.8°
θ = 68.1°
X
0
30
60
90
120
150
180
210
240
270
300
330
360
● From Schroeder et al. (1984) o = 13.5 x = 12.3

FIGURE 7.

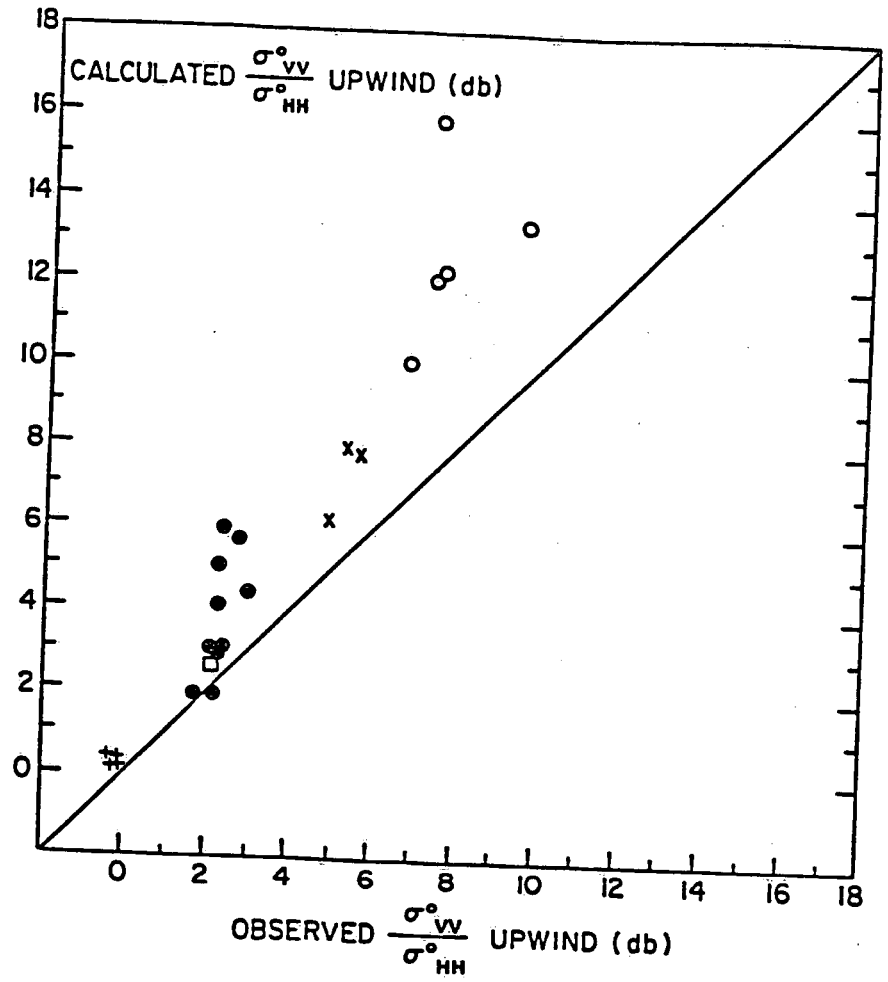
CALCULATED $\frac{\sigma^\circ_{VV}}{\sigma^\circ_{HH}}$ UPWIND (db)
OBSERVED $\frac{\sigma^\circ_{VV}}{\sigma^\circ_{HH}}$ UPWIND (db)
0
2
4
6
8
10
12
14
16
18

FIGURE 8.

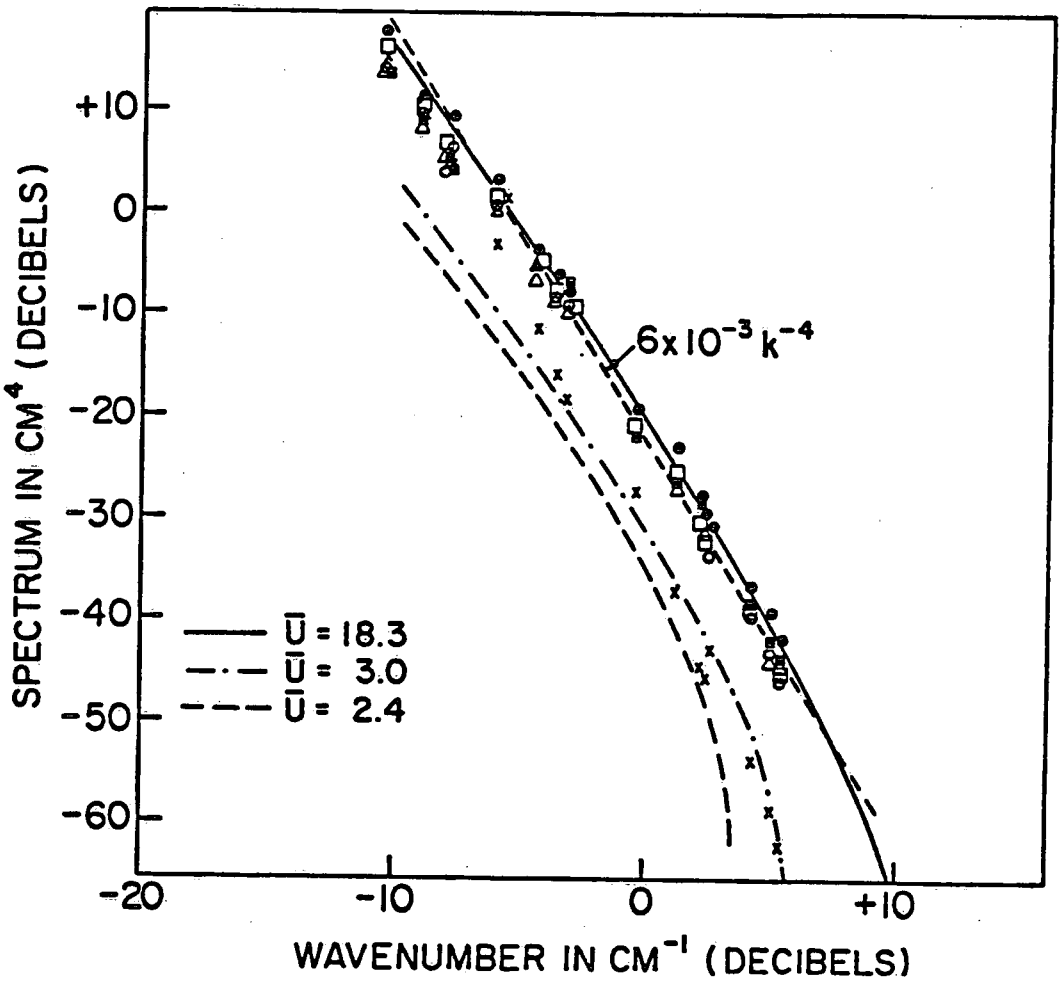
+10
0
-10
-20
-30
-40
-50
-60
-20
-10
0
+10
SPECTRUM IN CM⁴ (DECIBELS)
WAVENUMBER IN CM⁻¹ (DECIBELS)
6x10⁻³ k⁻⁴
U = 18.3
U = 3.0
U = 2.4

FIGURE 9.

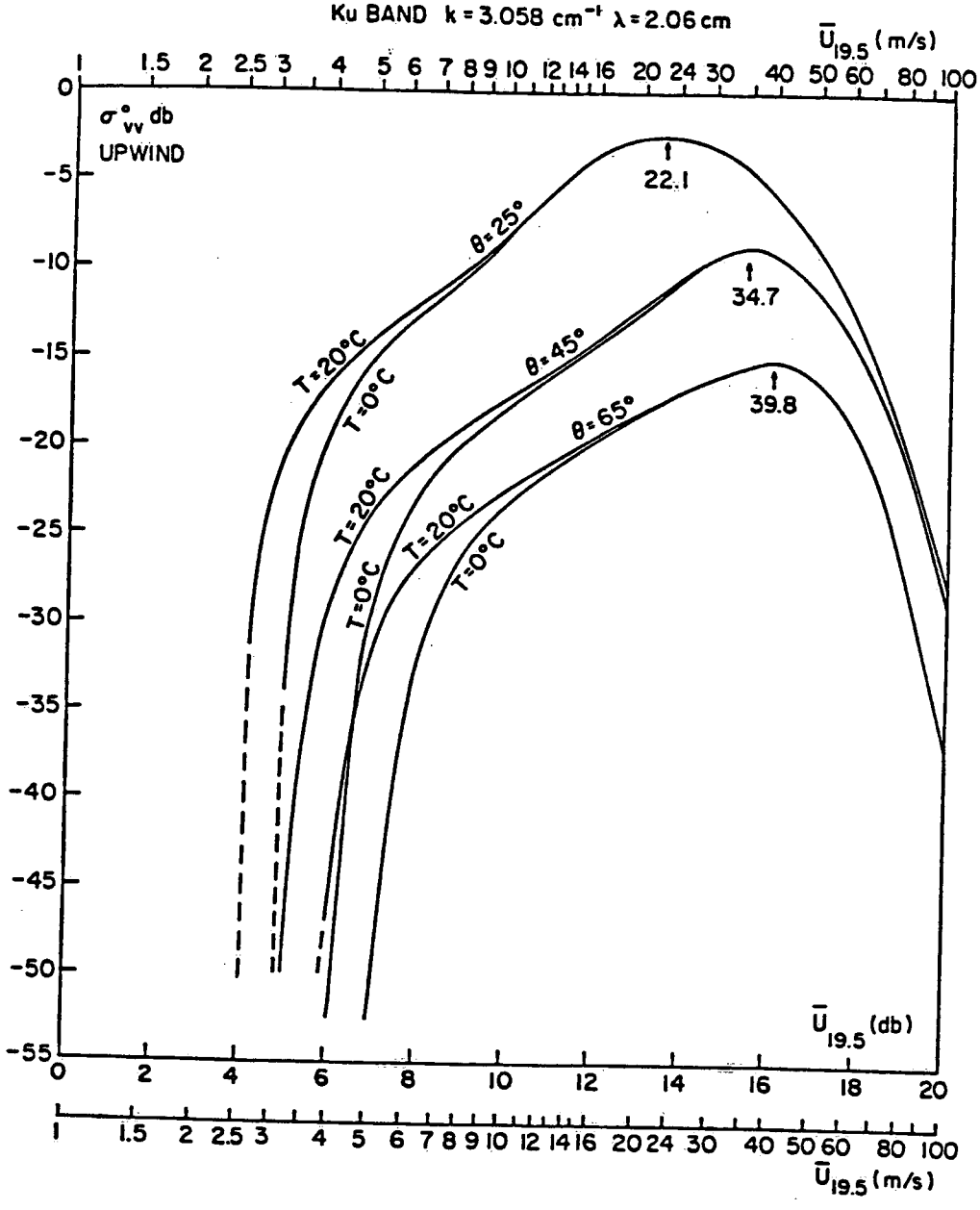
Ku BAND k = 3.058 cm⁻¹ λ = 2.06 cm
$\bar{U}_{19.5}$ (m/s)
1 1.5 2 2.5 3 4 5 6 7 8 9 10 12 14 16 20 24 30 40 50 60 80 100
0
-5
-10
-15
-20
-25
-30
-35
-40
-45
-50
-55
σ°_{vv} db
UPWIND
22.1
34.7
39.8
θ=25°
θ=45°
θ=65°
T=20°C
T=0°C
T=20°C
T=0°C
T=20°C
T=0°C
$\bar{U}_{19.5}$ (db)
0 2 4 6 8 10 12 14 16 18 20
1 1.5 2 2.5 3 4 5 6 7 8 9 10 12 14 16 20 24 30 40 50 60 80 100
$\bar{U}_{19.5}$ (m/s)

FIGURE 10.

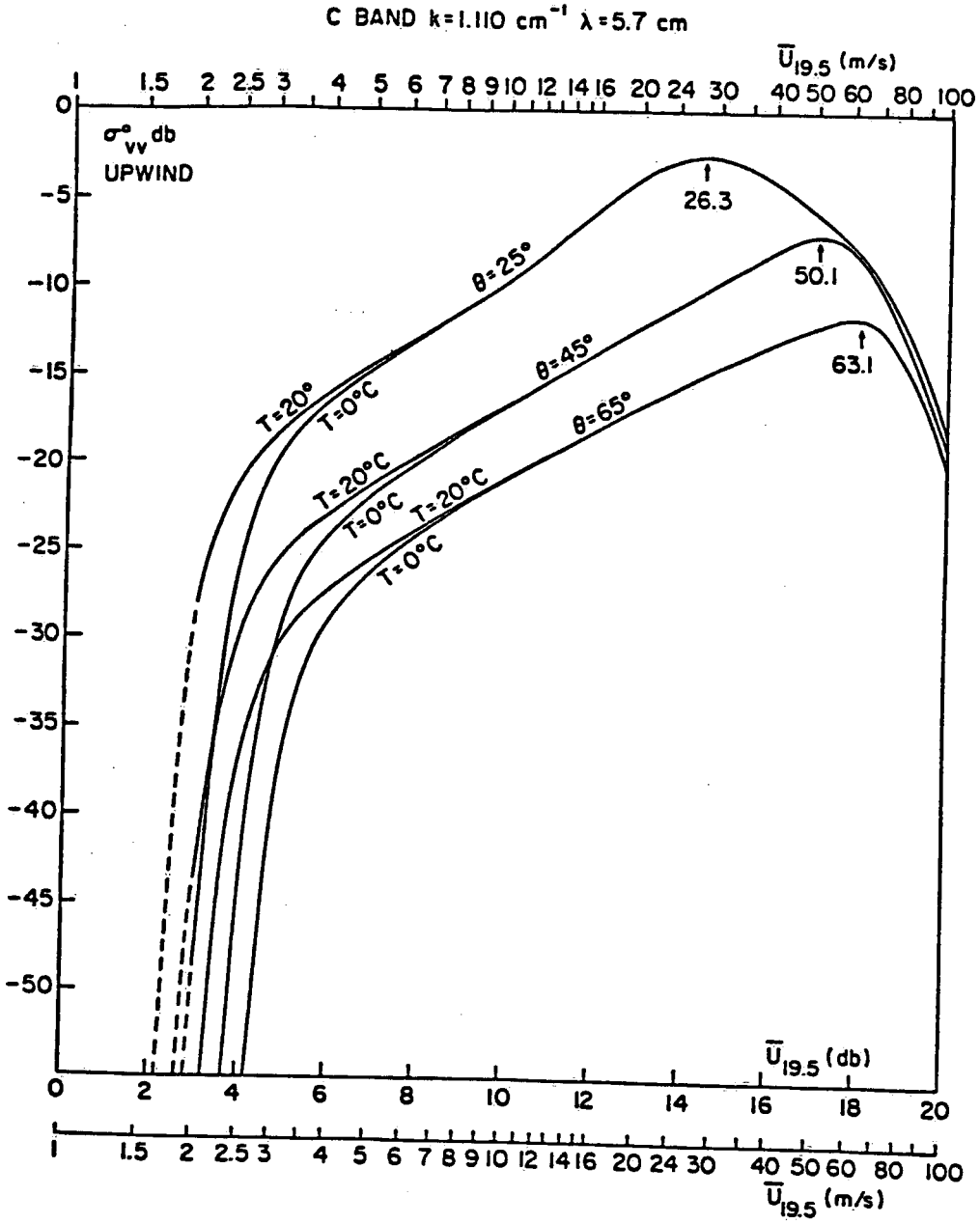
C BAND k=1.110 cm⁻¹ λ=5.7 cm
$\bar{U}_{19.5}$ (m/s)
1 1.5 2 2.5 3 4 5 6 7 8 9 10 12 14 16 20 24 30 40 50 60 80 100
σ^{o}_{vv} db
UPWIND
0
-5
-10
-15
-20
-25
-30
-35
-40
-45
-50
θ=25°
θ=45°
θ=65°
T=20°
T=0°C
T=20°C
T=0°C
T=20°C
T=0°C
26.3
50.1
63.1
$\bar{U}_{19.5}$ (db)
0 2 4 6 8 10 12 14 16 18 20
1 1.5 2 2.5 3 4 5 6 7 8 9 10 12 14 16 20 24 30 40 50 60 80 100
$\bar{U}_{19.5}$ (m/s)

FIGURE 11.

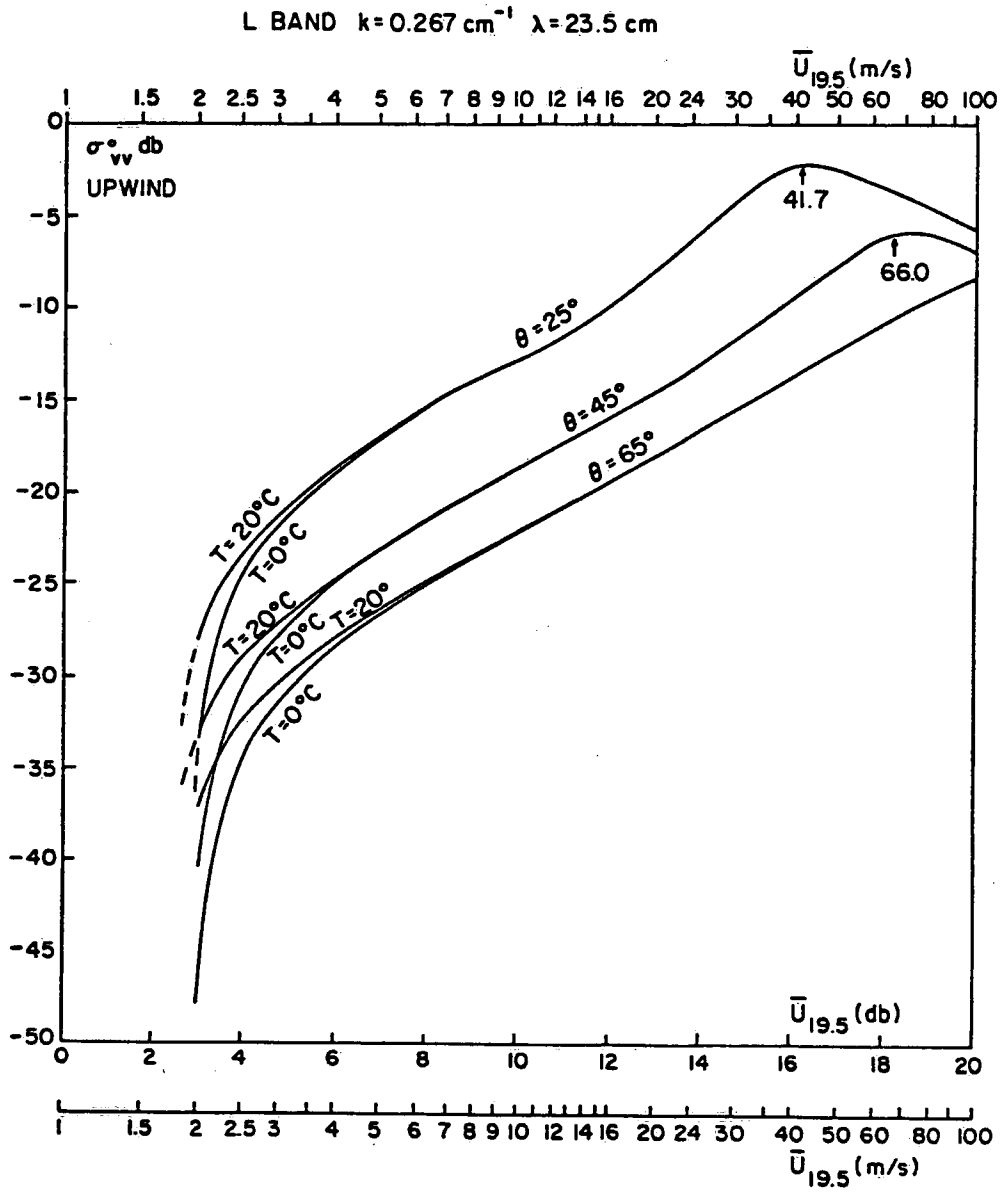
L BAND k=0.267 cm⁻¹ λ=23.5 cm
$\bar{U}_{19.5}$ (m/s)
1 1.5 2 2.5 3 4 5 6 7 8 9 10 12 14 16 20 24 30 40 50 60 80 100
0
-5
-10
-15
-20
-25
-30
-35
-40
-45
-50
σ°_{vv} db
UPWIND
41.7
66.0
θ=25°
θ=45°
θ=65°
T=20°C
T=0°C
T=20°C
T=0°C
T=20°
T=0°C
$\bar{U}_{19.5}$ (db)
0 2 4 6 8 10 12 14 16 18 20
1 1.5 2 2.5 3 4 5 6 7 8 9 10 12 14 16 20 24 30 40 50 60 80 100
$\bar{U}_{19.5}$ (m/s)

FIGURE 12.